MASTER THESIS

Leveraging Optical Lever Techniques for NEMS Resonators

A thesis submitted in partial fulfilment of the requirements for the degree of

Diplom-Ingenieur

in

Master's Program Embedded Systems

March 2025

Author:
Johannes Hiesberger
01604611

Institute:
Sensor and Actuator Systems

Supervisor:
Univ.Prof. Dr. Silvan Schmid

Co-Supervisors:
Dr. Hajrudin Bešić
Dr. Kostas Kanellopulos

Die approbierte gedruckte Originalversion dieser Diplomarbeit ist an der TU Wien Bibliothek verfügbar
The approved original version of this thesis is available in print at TU Wien Bibliothek.
TU Bibliothek Your knowledge hub WIEN

Declaration

I hereby declare and confirm that this thesis is entirely the result of my own original work. Where other sources of information have been used, they have been indicated as such and properly acknowledged. I further declare that this or similar work has not been submitted for credit elsewhere.

Vienna, March 6, 2025

Johannes Hiesberger

Die approbierte gedruckte Originalversion dieser Diplomarbeit ist an der TU Wien Bibliothek verfügbar
The approved original version of this thesis is available in print at TU Wien Bibliothek.

Die approbierte gedruckte Originalversion dieser Diplomarbeit ist an der TU Wien Bibliothek verfügbar
The approved original version of this thesis is available in print at TU Wien Bibliothek.

Kurzfassung

Die präzise Messung mechanischer Resonanzen in Systemen im Nanometerbereich (NEMS) ist sowohl für die Grundlagenforschung als auch für technologische Anwendungen von entscheidender Bedeutung. Verschiedene Read-out-Techniken zur Charakterisierung von Mikro- und Nanoresonatoren bieten jeweils spezifische Vor- und Nachteile. Interferometrische optische Methoden werden aufgrund ihrer hohen Empfindlichkeit häufig zur Messung von Auslenkungen eingesetzt.

Eine der frühesten optischen Read-out-Methoden ist die Optical Lever-Technik, die in verschiedenen Anwendungen erfolgreich genutzt wird. Aufgrund ihrer Einfachheit und Robustheit wird sie insbesondere in der Atomic Force Microscopy (AFM) verwendet, jedoch bisher nur begrenzt in anderen NEMS-Implementierungen. Jüngste Arbeiten zeigen, dass ein Optical Lever-System durch das Vermeiden von optischen Rückkopplungen eine Rauschgrenze erreichen kann, die zwei Größenordnungen unterhalb des Standard-Quantenlimits liegt.

Die begrenzte Anwendung und der Mangel an vergleichenden Analysen der Optical Lever-Technik für NEMS motivieren diese Arbeit. Diese Studie untersucht die Machbarkeit der Optical Lever-Technik für die Frequenzmessung von NEMS-Resonatoren. Zur Bewertung der Effektivität dieser Technik wird ein experimentelles Setup entwickelt, das einen direkten Vergleich mit zwei etablierten Messmethoden ermöglicht: (i) einem elektrischen Read-out mittels Magnetomotive-Technik und (ii) einer optischen Messung mit Laser Doppler Vibrometrie. Die Auswirkungen jeder Methode auf die Frequenzstabilität der Resonatoren werden unter vergleichbaren Bedingungen analysiert. Zusätzlich wird eine NEMS-Anwendung mit einer Read-out-Methode unter-

sucht, um die Leistungsfähigkeit der Optical Lever-Technik im Vergleich zur magnetomotiven Auslese zu bewerten. Die Ergebnisse zeigen, dass die Optical Lever-Technik eine mit interferometrischen Methoden vergleichbare Leistung erbringt und sich für Membran-NEMS eignet. Die erzielte Rauschperformance übertrifft die der elektrischen Auslese signifikant. Diese Erkenntnisse tragen zur weiteren Erforschung alternativer Transduktionsmechanismen für nano-mechanische Systeme bei und eröffnen neue Möglichkeiten für stabile und hochpräzise Sensortechnologien.

Die approbierte gedruckte Originalversion dieser Diplomarbeit ist an der TU Wien Bibliothek verfügbar
The approved original version of this thesis is available in print at TU Wien Bibliothek.
TU Bibliothek Your knowledge hub WIEN

Abstract

The precise measurement of mechanical resonances in nanoscale devices (NEMS) is critical for both fundamental research and technological applications. Various read-out techniques exist to characterize micro- and nanoscale resonators, each with distinct advantages and limitations. Among these, interferometric optical methods are widely used due to their high sensitivity in displacement measurements.

One of the earliest optical read-out methods is the optical lever technique, which has been successfully implemented in various applications. Its simplicity and robustness make it particularly useful in Atomic Force Microscopy (AFM), yet its adoption in other NEMS implementations remains limited. Recent studies have demonstrated that an optical lever system can mitigate optical back-action effects, achieving a read-out noise floor two orders of magnitude below the standard quantum limit.

The limited adoption and lack of comparative analysis of optical lever read-out techniques for NEMS motivate this study. This work investigates the feasibility of using the optical lever technique for frequency measurements of NEMS resonators. To evaluate the effectiveness of this approach, an experimental setup was designed to enable a direct comparison with two established measurement methods: (i) an electrical read-out technique, the magnetomotive read-out, and (ii) an optical read-out technique, the laser Doppler vibrometer. The impact of each method on the frequency stability of the resonators is assessed under comparable conditions. Additionally, a NEMS application utilizing a read-out scheme is selected to compare the performance of the optical lever technique and the magnetomotive read-out,

Die approbierte gedruckte Originalversion dieser Diplomarbeit ist an der TU Wien Bibliothek verfügbar
The approved original version of this thesis is available in print at TU Wien Bibliothek.
TU Bibliothek Your knowledge hub WIEN

demonstrating the impact of the optical method relative to the electrical approach.

The results confirm that the optical lever technique provides performance comparable to interferometric methods and is well-suited for membrane-based NEMS. The achieved noise performance surpasses that of the electrical read-out. These findings contribute to the ongoing exploration of alternative transduction mechanisms for nanoscale mechanical systems, offering a promising approach for stable and high-precision sensing applications.

Die approbierte gedruckte Originalversion dieser Diplomarbeit ist an der TU Wien Bibliothek verfügbar
The approved original version of this thesis is available in print at TU Wien Bibliothek.
TU Bibliothek Your knowledge hub WIEN

Acknowledgements

I would like to express my deepest gratitude to my advisor, **Professor Silvan Schmid**, for his invaluable guidance, continuous support, and insightful discussions throughout this research. His encouragement, positivity, and enthusiasm have played a crucial role in shaping this work.
I am also thankful to **Harjudin Bešić** for supervising this work and providing valuable input whenever needed. Additionally, I want to thank **Kostas Kanellopulos** for many late-night discussions and measurement sessions-you always pushed me to go all the way and achieve the best possible results.
To the members of the **MNS group**, I am grateful for all your helpful feedback, technical assistance, and the experiences and memories we shared. In particular I thank **Tatjana Penn** for your help in the fabrication of the resonators and the care you show for everyone around you.
Special thanks go to **Jelena Timarac Popović** and **Paolo Martini** for sharing the office with me through it all. You were always there to provide input, have a conversation or just to hear me out.
I also thank **Johannes Steurer** and **Maximilian Thier** for their help with the electronic circuits. You were always available to assist me in identifying and resolving mistakes.
Finally, I am deeply grateful to my family and friends for their unwavering support, patience, and encouragement. Their belief in me has been a constant source of motivation throughout this journey.
While I have made every effort to recognize those who have contributed to this work, I sincerely apologize if I have unintentionally overlooked anyone. I am truly grateful to everyone who has supported me, whether directly or indirectly, in completing this thesis.

Die approbierte gedruckte Originalversion dieser Diplomarbeit ist an der TU Wien Bibliothek verfügbar
The approved original version of this thesis is available in print at TU Wien Bibliothek.
TU Bibliothek Your knowledge hub WIEN

Contents

Declaration i

Kurzfassung ii

Abstract iv

1 State-of-the-Art 1

1.1 Nano-Electro-Mechanical-System . . . 3
1.2 Noise Analysis . . . 8
1.2.1 Allan-Deviation . . . 8
1.2.2 Noise sources . . . 9
1.3 Thermomechanical Noise Measurement . . . 12
1.4 Lock-in Amplifiers . . . 14
1.5 Phase-Locked Loop . . . 16
1.6 Optical Lever Technique . . . 18
1.6.1 Estimation of expected amplitude . . . 19
1.7 Laser Doppler Vibrometer . . . 25
1.8 Fourier-Transform-Infrared-Spectroscopy . . . 26

2 Methods 28

2.1 NEMS Resonator . . . 29
2.2 Optical Lever Setup . . . 31
2.2.1 Photodiode Circuit . . . 35
2.2.2 Measurement Procedure . . . 38
2.3 Magnetomotive Technique Setup . . . 41

Die approbierte gedruckte Originalversion dieser Diplomarbeit ist an der TU Wien Bibliothek verfügbar
The approved original version of this thesis is available in print at TU Wien Bibliothek.
TU Bibliothek Your knowledge hub WIEN

2.3.1 Measurement Procedure 42
2.4 Laser Doppler Vibrometer Technique Setup 42
2.4.1 Measurement Procedure 43
2.5 FTIR Measurement Setup 44

3 Results **46**
3.1 Allan Variance 47
3.1.1 Optical Lever vs Laser Vibrometer 47
3.1.2 Optical Lever vs Magnetomotive 55
3.2 FTIR Spectra 59

4 Conclusion **68**

Bibliography **71**

Die approbierte gedruckte Originalversion dieser Diplomarbeit ist an der TU Wien Bibliothek verfügbar
The approved original version of this thesis is available in print at TU Wien Bibliothek.

Die approbierte gedruckte Originalversion dieser Diplomarbeit ist an der TU Wien Bibliothek verfügbar
The approved original version of this thesis is available in print at TU Wien Bibliothek.

Chapter 1

State-of-the-Art

Nano-Electro-Mechanical Systems (NEMS) are utilized in a wide range of applications, and various read-out techniques have been developed to study and characterize them [1–5], each offering distinct advantages and limitations. Among these, interferometric optical techniques have been widely used to measure displacement with high sensitivity [2]. The low detection noise of optical techniques is a particularly important characteristic, especially for resonators with high quality factors [6, 7].

As one of the earliest optical read-out approaches [8], the optical lever technique has been implemented in various applications [9–12], with its simplicity in design making it highly robust [13]. Putman et al. not only highlights the straightforward nature of the optical lever technique compared to interferometric approaches, but also demonstrates that both methods share the same fundamental detection limits [13].

Despite its success in Atomic Force Microscopy (AFM), which primarily relies on cantilevers, this method has not been widely applied to other NEMS devices compared to interferometric techniques. Recent work by Hao et al. uses membrane-based NEMS and demonstrates that an optical lever system can evade back-action caused by optical forces, achieving a read-out noise floor two orders of magnitude lower than the standard quantum limit [14].

The lack of widespread implementations and comparative analyses of optical lever read-out techniques for NEMS motivates further exploration. This work

investigates the feasibility of using the optical lever technique for frequency measurements of NEMS resonators. To evaluate the effectiveness of this approach, an experimental setup was designed to enable a direct comparison with two established measurement methods: (i) an electrical read-out technique, the magnetomotive read-out, and (ii) an optical read-out technique, the laser Doppler vibrometry (LDV). Using the same NEMS resonators under comparable conditions, the impact of each method on the frequency stability of the resonators is assessed.

Furthermore, a NEMS application utilizing a read-out scheme was selected to compare the performance of the optical lever technique and the magnetomotive read-out, demonstrating the impact of the optical method relative to the electrical approach.

This study not only evaluates the feasibility of using an optical lever for membrane-based NEMS but also highlights its potential advantages in terms of stability. The findings contribute to the broader exploration of alternative transduction mechanisms for nanoscale mechanical systems, paving the way for more versatile and optimized sensing technologies.

Die approbierte gedruckte Originalversion dieser Diplomarbeit ist an der TU Wien Bibliothek verfügbar
The approved original version of this thesis is available in print at TU Wien Bibliothek.
TU Bibliothek Your knowledge hub WIEN

1.1 Nano-Electro-Mechanical-System

Nanoelectromechanical systems (NEMS) are miniaturized mechanical devices that integrate electrical and mechanical properties at the nanoscale. They represent the natural evolution of microelectromechanical systems (MEMS), but at an even smaller scale. Due to their small mass and high surface-to-volume ratio, NEMS are widely used in ultra-sensitive mass sensing, light detection, and spectroscopy. One of the fundamental aspects of most NEMS is their vibrational behavior, which is crucial for understanding their mechanical properties and optimizing their performance in sensing and actuation. As with all mechanical systems, NEMS exhibit characteristic vibration modes defined by their geometry and material properties. These vibrational modes define how energy is stored and transferred within the system. Every continuous mechanical system has vibrational frequencies in which the kinetic energy of the vibration is equal to the potential energy stored within the deformation. When considering a model without energy loss, these frequencies are referred to as eigenfrequencies. Energy seamlessly transitions between potential and kinetic states in this system, perpetually, unless affected by an external force. In contrast, a real-world structure dissipates energy with each oscillation cycle due to inherent damping. For structures affected by this loss, resonance frequencies can be determined. While these resonance frequencies take damping into account, the eigenfrequencies disregard any form of damping and can be calculated through analytical techniques or approximated through simulations like the finite element method (FEM). Consequently, the resonance frequencies can also be estimated, as they are known to be slightly lower than the corresponding eigenfrequency for the same model due to damping [15].

Figure 1.1a shows an ideal model of a resonance in amplitude and phase as a function of frequency. In comparison, Figure 1.1b depicts the resonance of a real NEMS, recorded using a laser Doppler vibrometer (LDV). While the measurement contains noise that the model lacks, the general shape remains the same. The amplitude exhibits a peak at the resonance frequency, where

Die approbierte gedruckte Originalversion dieser Diplomarbeit ist an der TU Wien Bibliothek verfügbar
The approved original version of this thesis is available in print at TU Wien Bibliothek.
TU Bibliothek Your knowledge hub WIEN

the same amount of input energy results in a significantly higher measured amplitude. Another characteristic of resonance is observed in the phase of the signal, where the measured phase undergoes a total 180° shift before and after the resonance.

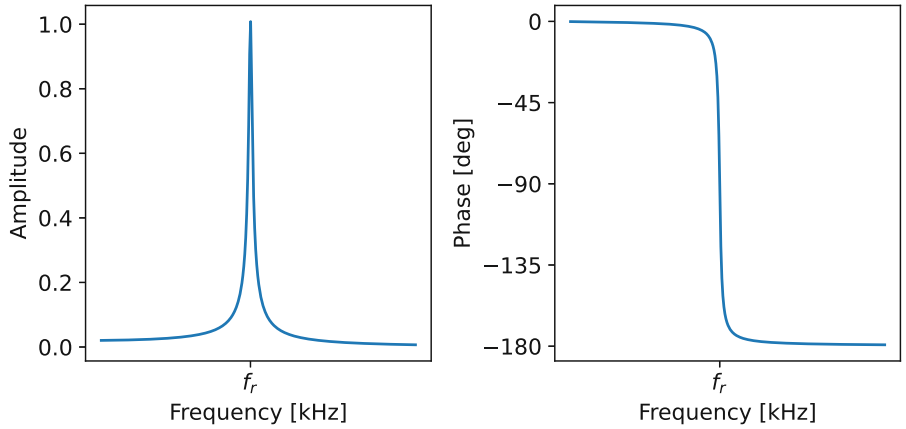

(a) Representative resonance behavior in amplitude and phase

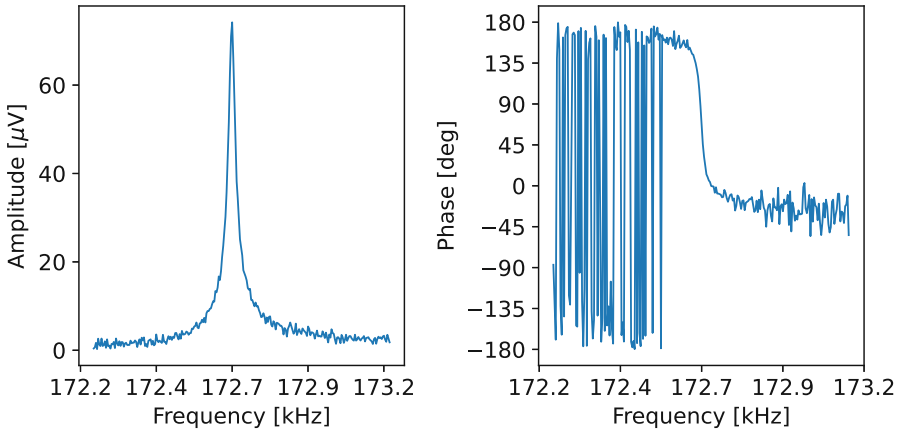

(b) Amplitude and phase of a resonance measured with a laser Doppler vibrometer.

Figure 1.1: Comparison of an ideal and measured resonance

Each eigenfrequency corresponds to a unique mode shape, depicting the periodic deformation pattern exhibited by the structure at that distinct fre-

Die approbierte gedruckte Originalversion dieser Diplomarbeit ist an der TU Wien Bibliothek verfügbar
The approved original version of this thesis is available in print at TU Wien Bibliothek.
TU Bibliothek Your knowledge hub WIEN

quency. When analyzing the vibration along a single axis, certain key features emerge: some areas remain stationary, known as nodes, while others undergo maximal displacement, referred to as anti-nodes.

For specific structures, analytical solutions for the eigenfrequencies are known. In the case of this work rectangular membranes are used and a solution for their eigenfrequencies can be found that is based on parameters such as dimensions, material stress, and density of the membrane exists. The resonance frequency can then be estimated based on the eigenfrequency and the expected damping. For this work, the modes observed are only out-of-plane modes, but it should be mentioned that more types of modes, like torsional and in-plane modes exist. A rectangular membrane has two defining lengths for out-of-plane modes, which in turn define its eigenmodes. These modes are distinguished by the count of anti-nodes (local maxima), and given the two dimensions, the distinction between the modes is facilitated by two distinct numbers. Depending on this count of anti-nodes, the equation for eigenmodes of a membrane can be found, which is given in Equation (1.1) [15].

$$\omega_{n,j} = \sqrt{\frac{\sigma}{\rho}} \sqrt{\frac{n^2\pi^2}{L_x^2} + \frac{j^2\pi^2}{L_y^2}} \tag{1.1}$$

$\omega_{n,j}$ represents a specific eigenfrequency in rad and i and j are indices of the mode of this eigenfrequency. L_x and L_y are the respective lengths of the membrane in its two dimensions, ρ is the density of the material, and σ is the tensile stress of the membrane. The equation shows that variations in stress lead to changes in the eigenfrequency and, consequently, the resonance frequency. Since the stress depends on factors such as temperature, pressure, and external forces, the resonance frequency is inherently sensitive to these parameters. This dependence enables resonators to be utilized in a wide range of applications.

Figure 1.2 shows the modeshapes for the six lowest eigenfrequencies of a square membrane, once measured with an LDV and once calculated using modeshapes according to [15]. It has to be mentioned, that since this is a square membrane that the modeshapes are symmetrical and for each mode

Die approbierte gedruckte Originalversion dieser Diplomarbeit ist an der TU Wien Bibliothek verfügbar
The approved original version of this thesis is available in print at TU Wien Bibliothek.
TU Bibliothek Your knowledge hub WIEN

depicted here there exists another mode for which the modeshape is rotated by 90°.

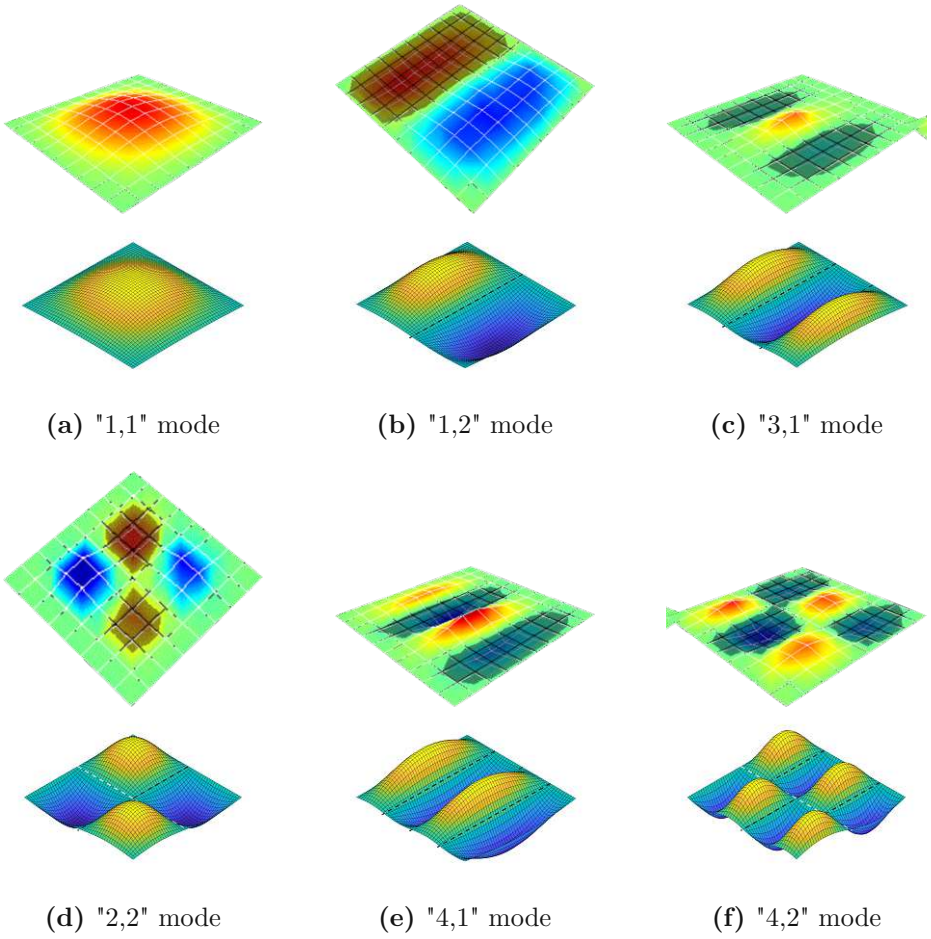

(a) "1,1" mode **(b)** "1,2" mode **(c)** "3,1" mode

(d) "2,2" mode **(e)** "4,1" mode **(f)** "4,2" mode

Figure 1.2: Modeshapes of a square membrane (top measured, bottom analytical solution).

In cases where the structure deviates from the straightforward analytical solution or where there is limited knowledge of the composition and material properties of a resonator, determining resonance frequencies requires an empirical approach. To find resonance frequencies, the actuation and read-out of a system must have been established. If there is a way to excite the mode of interest and also a way to measure said mode, the frequency of the actuation can be changed over a range of frequencies while the output is observed.

Die approbierte gedruckte Originalversion dieser Diplomarbeit ist an der TU Wien Bibliothek verfügbar
The approved original version of this thesis is available in print at TU Wien Bibliothek.
TU Bibliothek Your knowledge hub WIEN

When the frequency of the actuation coincides with the resonance frequency, the measured amplitude is significantly higher than when they do not match. With a sufficiently wide range, depending on the resonator and the read-out scheme, multiple resonances can be observed, as shown in Figure 1.3.

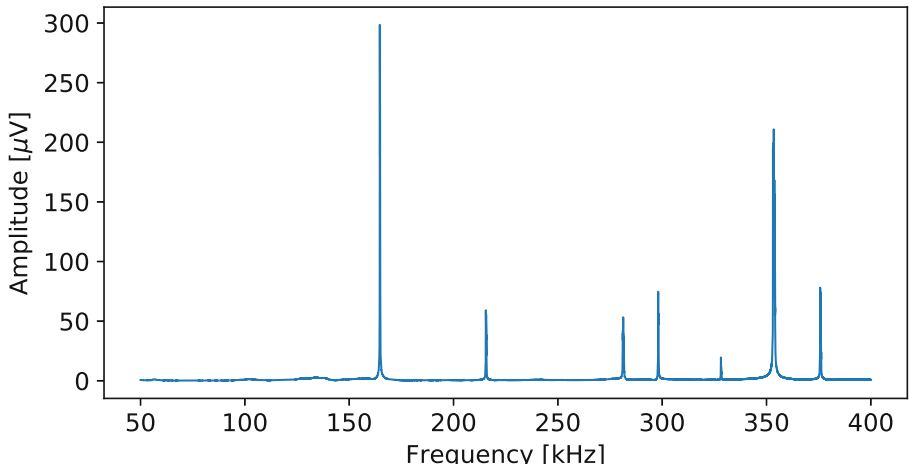

Figure 1.3: Frequency sweep of a membrane resonator measured with an LDV.

For this particular resonator, the first observable resonance frequency is approximately at 170 kHz, followed by several higher modes at higher frequencies. A read-out might fail to observe certain resonance frequencies depending on the location on the resonator where the oscillation amplitude is measured. For example, an optical read-out measuring displacement is usually focused on a specific spot on the structure, and if this spot happens to be a node of the mode shape, no displacement is detected. The same limitation applies to electrical read-outs due to the symmetry of the vibration. Therefore, not every resonance frequency can be observed with every setup.

Die approbierte gedruckte Originalversion dieser Diplomarbeit ist an der TU Wien Bibliothek verfügbar
The approved original version of this thesis is available in print at TU Wien Bibliothek.
TU Bibliothek Your knowledge hub WIEN

1.2 Noise Analysis

1.2.1 Allan-Deviation

Allan variance, named after David W. Allan, is a statistical measure crucial for analyzing frequency stability in systems like clocks and oscillators. It is particularly suited for distinguishing various noise types and their contribution, specifically providing a more reliable metric than classical variance.
The Allan variance, denoted as $\sigma_y^2(\tau)$, is the mean square of the differences between successive averaged measurements of a magnitude y, taken over a period τ. It is mathematically expressed as:

$$\sigma_y^2(\tau) = \frac{1}{2(N-1)} \sum_{i=1}^{N-1} (y_{i+1,\tau} - y_{i,\tau})^2 \tag{1.2}$$

where $y_{i,\tau}$ represents the i^{th} measurement of y averaged over time τ.
In the context of resonance-based sensors, the Allan variance is applied to the normalized instantaneous frequency difference from the natural frequency of the resonator, given by:

$$y(t) = \frac{\omega(t) - \omega_n}{\omega_n} \tag{1.3}$$

where $\omega(t)$ is the instantaneous frequency, and ω_n is the natural frequency. The Allan variance is part of a broader set of time-domain measurements used for frequency accuracy characterization. The frequency-domain analysis involves the single-sided fractional frequency noise power spectral density $S_y(\omega)$, encompassing various noise components like thermomechanical/transduction noise and thermal fluctuations. In practical scenarios, the Allan variance is favored in the sensing community for directly estimating system noise over a given integration time.
The Allan deviation σ_y is simply the square root of the Allan variance. This makes it more intuitive since its unit is the same as the original frequency, which it is based on [15, 16].

Die approbierte gedruckte Originalversion dieser Diplomarbeit ist an der TU Wien Bibliothek verfügbar
The approved original version of this thesis is available in print at TU Wien Bibliothek.

1.2.2 Noise sources

Understanding and characterizing various noise sources is crucial to optimizing the performance of NEMS. The Allan deviation serves as a sensitive gauge, highlighting the noise characteristics of such systems since different types of noise manifest at various timescales and influence the stability of these devices in distinct ways. Figure 1.4 shows a representation of different types of noise and how they show in an Allan deviation of an actual resonator.

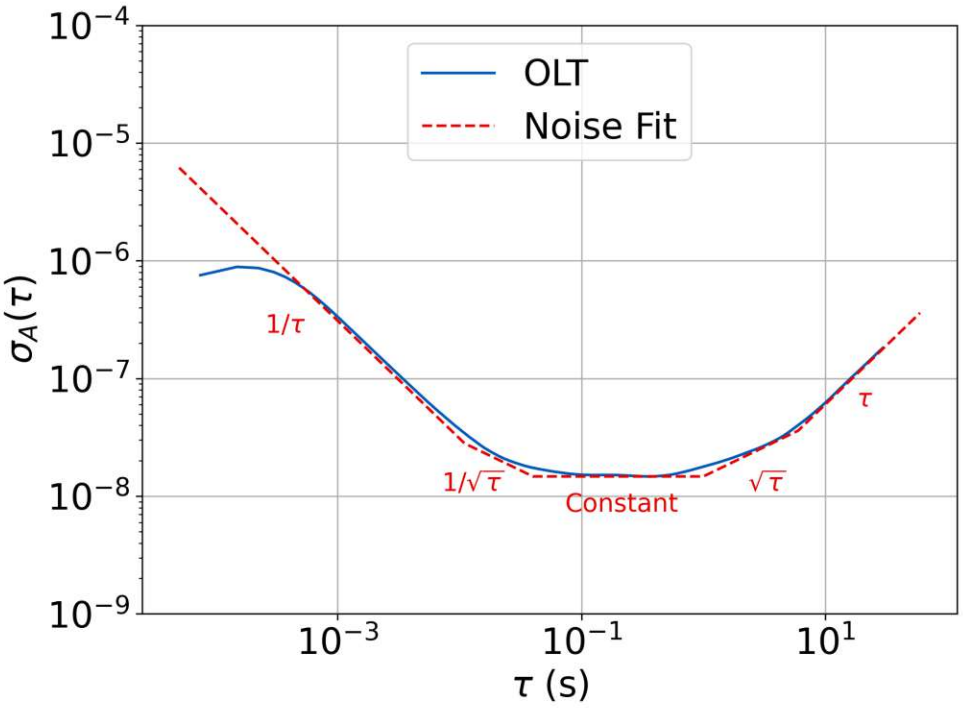

Figure 1.4: Allan deviation of a resonator fit with the theoretical noise slopes.

The white phase noise and flicker phase noise component causes the Allan deviation to decrease rapidly with averaging time, following a $\frac{1}{\tau}$ slope. This means that as more data points are averaged, the stability improves very quickly. White phase noise is dominant at very short timescales, typically

Die approbierte gedruckte Originalversion dieser Diplomarbeit ist an der TU Wien Bibliothek verfügbar
The approved original version of this thesis is available in print at TU Wien Bibliothek.

introduced by electronic thermal noise. Since it averages out efficiently, it does not significantly affect long-term stability [16].

The white frequency noise results in an Allan deviation that decreases as $\frac{1}{\sqrt{\tau}}$, indicating that stability improves over time, though at a slower rate compared to phase noise. This type of noise arises from random fluctuations in the frequency source and typically dominates at medium averaging times. White frequency noise is fundamental in many systems, as it represents uncorrelated random variations in the frequency output. In NEMS devices, this noise characterizes the intrinsic behavior of the mechanical resonator. While other noise sources reflect contributions from the entire system, including the readout electronics and environmental influences, this region of the Allan deviation plot provides insight into the resonator itself, independent of external factors [16, 17].

The flicker frequency, or 1/f noise, noise produces an Allan deviation contribution that remains constant with increasing averaging time, following a constant trend. This indicates that stability does not improve with further averaging, as the fluctuations follow a power-law behavior that resists cancellation. Flicker frequency noise is often attributed to long-term instabilities in oscillator electronics, such as aging effects or environmental influences [15, 16].

The random walk frequency noise causes the Allan deviation to increase with averaging time, following a $\sqrt{\tau}$ slope. This means that as the observation time grows, the frequency stability worsens due to slow, unpredictable drifts in the system. This type of noise is commonly introduced by external environmental effects, such as temperature changes or mechanical stress, and becomes dominant at very long averaging times. Since it does not average out, it represents a fundamental limitation in long-term oscillator performance [16].

Another type of noise is drift, which has is a consistent change in frequency. This drift is caused by factors such as temperature stabilization, pressure changes, material relaxation, and other environmental influences. These slow frequency changes follow a τ slope. While the impact of slow drifts is minimal for short integration times, it becomes increasingly apparent as the integration time increases [6, 15, 16].

Die approbierte gedruckte Originalversion dieser Diplomarbeit ist an der TU Wien Bibliothek verfügbar
The approved original version of this thesis is available in print at TU Wien Bibliothek.
TU Bibliothek Your knowledge hub WIEN

For this work these types of noise are grouped together for simplicity.

Thermomechanical noise is a white frequency noise caused by the random vibrational motion of mechanical structures, which itself results from the interaction of thermal energy with the intrinsic properties of the material. These fluctuations arise from thermal energy present at any temperature above 0 K and characterize the inherent noise performance of the resonator.

Detection or **transduction noise** primarily consists of shot noise, Johnson-Nyquist noise, and flicker noise, all of which introduce random fluctuations in measurement signals. Compared to thermomechanical noise, this type of noise includes components originating from the electronics in the system. Oftentimes the detection noise is so significant that it covers the thermomechanical noise.

Drift is dominated by slow frequency drifts and random walk frequency noise, leading to long-term stability issues as environmental factors induce slow, unpredictable changes in system behavior.

For laser-based systems, it is also useful to consider intensity fluctuations of the laser itself, as power variations affect the resonator via **photo-thermal back-action**. In this process, the resonator absorbs light, and the absorbed energy alters its mechanical properties. Depending on the laser intensity and the absorption characteristics of the material, this effect can become a dominant source of noise [6, 17, 18].

Die approbierte gedruckte Originalversion dieser Diplomarbeit ist an der TU Wien Bibliothek verfügbar
The approved original version of this thesis is available in print at TU Wien Bibliothek.
TU Bibliothek Your knowledge hub WIEN

1.3 Thermomechanical Noise Measurement

At the heart of thermomechanical noise is the thermal motion of atoms or molecules in any material at a non-zero temperature. This motion, comprised of vibrations and collisions, appears random but is driven by thermal energy. Due to the resonance frequencies in mechanical structures, the system tends to oscillate even without external actuation and just based on the internal energy of the material. This effect is especially significant for small structures like NEMS. This is called the thermomechanical resonance and depending on the damping, noise in the system and method of measurement, these resonances can be observed. This is quite significant to note, since that means one can pick up a resonance frequency without specifically exciting the structure, it is visible just based on its temperature. Thermomechanical resonances are especially important because they allow the identification of system characteristics without any deviations that might come with a driven system [15]. One of the most identifiable features of thermomechanical resonance is a peak in the response of the system, at the resonant frequency. One example of such a thermomechanical resonance is shown in Figure 1.5, which was recorded using an LDV, a spectrum analyzer and a membrane resonator. The reason a spectrum analyzer is used specifically, is to ensure the independence of the result to resolution measurement bandwidth. Figure 1.5 shows the data points in blue that represent the actual measurement, but to characterize this peak properly a fit is applied. The fit consists of two components, a constant PSD and a Lorentzian function, that once combined, fit the data well.

Die approbierte gedruckte Originalversion dieser Diplomarbeit ist an der TU Wien Bibliothek verfügbar
The approved original version of this thesis is available in print at TU Wien Bibliothek.

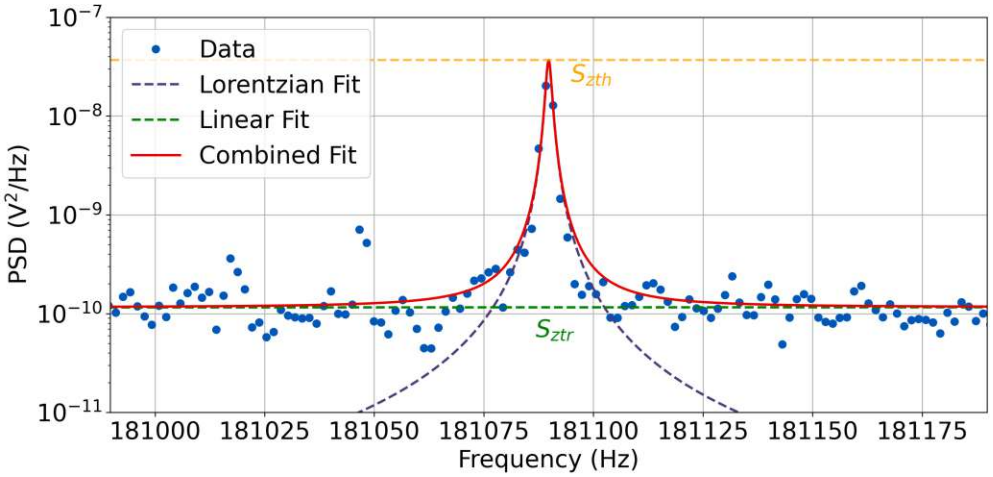

Figure 1.5: Thermomechanical noise peak measured with an LDV and fitted with a Lorentzian function

.

An important application of measuring the thermomechanical noise peak is the calibration of the system [15]. Essentially, by measuring the peak value of the resonance S_{zth} as well as the noise floor S_{tr}, a transduction coefficient κ_d can be calculated (equ. (1.4)).

$$\kappa_d = \sqrt{\frac{S_{ztr}}{S_{zth}}} \tag{1.4}$$

This transduction coefficient represents the ability of a read-out approach to resolve the thermomechanical noise peak in comparison to the noise floor. The lower the transduction coefficient the higher the thermomechanical noise peak in comparison to the noise floor [6].

Die approbierte gedruckte Originalversion dieser Diplomarbeit ist an der TU Wien Bibliothek verfügbar
The approved original version of this thesis is available in print at TU Wien Bibliothek.

1.4 Lock-in Amplifiers

Lock-in amplifiers are instruments often used in experimental physics and engineering applications to extract weak signals from noisy backgrounds. Their principle of operation relies on phase-sensitive detection, allowing for the precise measurement of signals buried in noise.

At the heart of a lock-in amplifier is a reference signal generator, typically a stable oscillator producing a sinusoidal signal. This reference signal is denoted as $V_{\text{ref}}(t) = V_0 \cos(\omega_{ref} \cdot t + \phi_{ref})$, where V_0 is the amplitude, ω_{ref} the angular frequency, t the time, and ϕ_{ref} represents the phase. The signal to be measured is also defined as a sinusoidal signal but with an arbitrary phase, amplitude and frequency $V_{\text{sig}}(t)$ (equ. (1.5)) [19].

$$\begin{aligned} V_{\text{ref}}(t) &= V_0 \sin(\omega_{\text{ref}} \cdot t + \phi_{\text{ref}}) \\ V_{\text{sig}}(t) &= V_0 \sin(\omega_{\text{sig}} \cdot t + \phi_{\text{sig}}) \end{aligned} \tag{1.5}$$

The multiplication of the two signals is shown in Equation (1.6).

$$\begin{aligned} V_{\text{ref}}(t) \cdot V_{\text{sig}}(t) &= V_0 \sin(\omega_{\text{ref}} \cdot t + \phi_{\text{ref}}) \cdot V_0 \sin(\omega_{\text{sig}} \cdot t + \phi_{\text{sig}}) \\ &= \frac{V_0^2}{2} \big[\cos((\omega_{\text{ref}} - \omega_{\text{sig}}) \cdot t + (\phi_{\text{ref}} - \phi_{\text{sig}})) \\ &\quad - \cos((\omega_{\text{ref}} + \omega_{\text{sig}}) \cdot t + (\phi_{\text{ref}} + \phi_{\text{sig}}))\big] \end{aligned} \tag{1.6}$$

The significance of this multiplication is apparent when the two frequencies, ω_{ref} and ω_{sig}, are equal. In this case, a signal at twice the frequency, at $2 \cdot \omega_{ref}$, and a DC (0 Hz) component are generated. By using a low-pass filter slightly above DC, the desired signal can be precisely isolated while eliminating noise at higher frequencies. This approach is sufficient for many applications; however, it neglects the phase difference between the signals. Although there is no issue if the signals are perfectly in phase, in all other cases, a dependency arises. To measure both amplitude and phase, a single sinusoidal reference signal is not sufficient. Instead, a second reference signal,

Die approbierte gedruckte Originalversion dieser Diplomarbeit ist an der TU Wien Bibliothek verfügbar
The approved original version of this thesis is available in print at TU Wien Bibliothek.
TU Bibliothek Your knowledge hub WIEN

phase-shifted by 90°, denoted as $Y(t)$, is introduced in conjunction with the original signal now depicted as $X(t)$ in Equation (1.7) and (1.8).

$$X(t) = V_0 \sin(\omega_{\text{ref}} \cdot t + \phi_{\text{ref}}) \cdot V_0 \cos(\omega_{\text{sig}} \cdot t + \phi_{\text{sig}}) \tag{1.7}$$

$$Y(t) = V_0 \sin(\omega_{\text{ref}} \cdot t + \phi_{\text{ref}}) \cdot V_0 \sin(\omega_{\text{sig}} \cdot t + \phi_{\text{sig}}) \tag{1.8}$$

$$A = \sqrt{X(t)^2 + Y(t)^2} \tag{1.9}$$

$$\Phi = \arctan\left(\frac{Y(t)}{X(t)}\right) \tag{1.10}$$

Utilizing the quadrature components in equation (1.9) and (1.10) enables lock-in amplifiers to measure not only with very low noise, but also phase-insensitive [19].

Die approbierte gedruckte Originalversion dieser Diplomarbeit ist an der TU Wien Bibliothek verfügbar
The approved original version of this thesis is available in print at TU Wien Bibliothek.
TU Bibliothek Your knowledge hub WIEN

1.5 Phase-Locked Loop

Phase-locked Loops (PLLs) are versatile control systems commonly employed in electronics and communications to synchronize the phase and frequency of an output signal with that of a reference signal. The core functionality of a PLL revolves around maintaining a stable phase relationship between these signals, making them invaluable in numerous applications, including frequency synthesis, signal clocks, demodulation and keeping track of frequency changes.

At the heart of a PLL lies a phase detector according to eq. 1.10, a component that compares the phase of the input signal with that of the reference signal. The phase detector generates an error signal proportional to the phase difference between the two signals. This error signal is then fed into a loop filter, which smoothens and conditions it before being used to adjust the frequency and phase of a controlled oscillator (CO). The CO generates an output signal whose frequency and phase are controlled by the feedback loop [6, 20].

A simple schematic of this process is shown in Figure 1.6. The frequency divider is an optional component that is used if there is a need to use a fraction of the original output frequency.

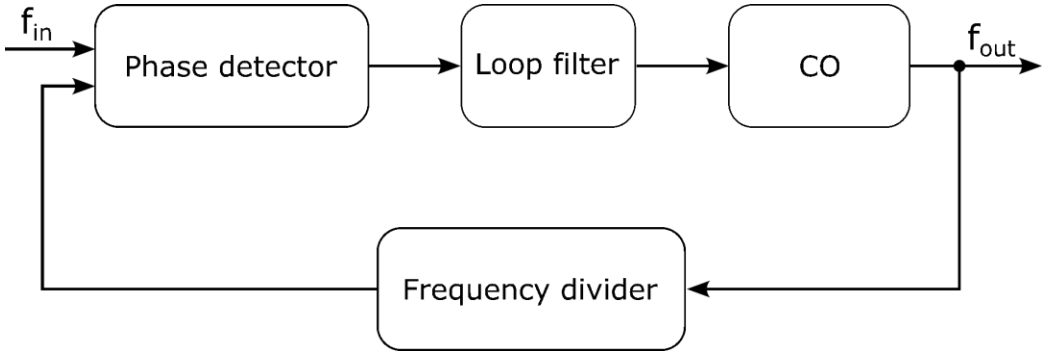

Figure 1.6: Schematic of a simple PLL

As the loop operates, the output signal of the CO is continuously adjusted to minimize the phase difference between the input and reference signal. Once

Die approbierte gedruckte Originalversion dieser Diplomarbeit ist an der TU Wien Bibliothek verfügbar
The approved original version of this thesis is available in print at TU Wien Bibliothek.

locked, the output signal tracks the frequency and phase of the reference signal, maintaining a stable phase relationship over time. PLL-based frequency tracking systems utilize the inherent resonance of NEMS to lock the phase and frequency of the output signal to a stable reference signal. By continuously adjusting the frequency of the drive, based on the phase difference between the readout and the reference signal, the PLL ensures that the reference signal remains in sync with the output signal of the NEMS resonator, effectively tracking any changes in the resonance frequency of the NEMS device [6].

Phase-locked loops and lock-in amplifiers are connected via their shared principle of phase detection through signal modulation. While lock-in amplifiers utilize phase-sensitive detection to extract and amplify signals buried in noise, PLLs focus on maintaining a precise phase and frequency relationship between input and reference signals.

Die approbierte gedruckte Originalversion dieser Diplomarbeit ist an der TU Wien Bibliothek verfügbar
The approved original version of this thesis is available in print at TU Wien Bibliothek.
TU Bibliothek Your knowledge hub WIEN

1.6 Optical Lever Technique

The optical lever technique (OLT) is based on light being deflected from an angled surface and the reflected beam path being displaced because of it. A simple depiction of this can be seen in Figure 1.7, where the angle of the surface in regards to the incident beam results in a displacement of the reflected beam depending on the original angle and the distance the reflected beam is able to travel.

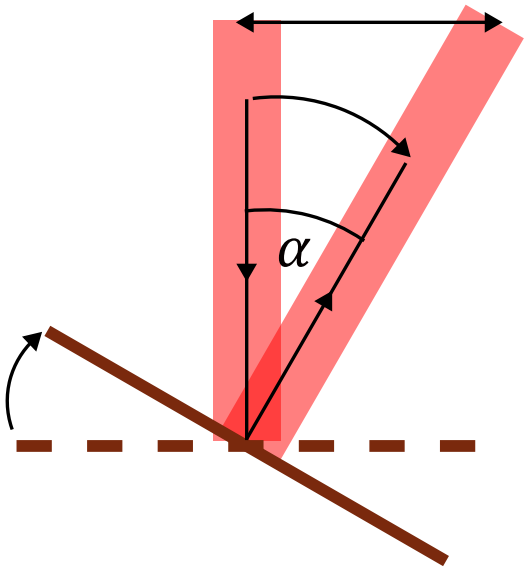

Figure 1.7: A change in angle of the reflective surface causes a displacement of the beam.

In the application of a read-out for NEMS, this angle change is due to the mode shape of a resonator at resonance. A laser beam is focused onto the surface of the NEMS, ideally at a nodal point of the mode shape, as this is the location where the resonance results in the highest change in angle and deflected based on the oscillation of the resonance. Depending on the structure and resonance, these nodal points occur at different positions. However, significant angle changes typically occur near the clamping of the resonator. The focused light is then reflected off the surface of the resonator, and since the structure moves and bends, the angle of reflection of the laser beam

Die approbierte gedruckte Originalversion dieser Diplomarbeit ist an der TU Wien Bibliothek verfügbar
The approved original version of this thesis is available in print at TU Wien Bibliothek.

changes. This change in reflection angle is typically very small, but using the optical lever, this angle change results in a displacement of the reflected laser beam that also depends on the distance it travels. Therefore, the longer the distance the beam travels after being deflected, the more pronounced the displacement of the beam. As a trade off, the longer the light travels the more diffracted it becomes and the harder it is to extract information [21]. This reflected beam position can then be detected via a position-sensitive photodetector, such as a quadrant photodiode. Assuming a quadrant photodiode, the center of the detector would be aligned to the reflected beam, producing the same signal for all photodiodes. Once the resonator oscillates, the beam hits the angled surface and is deflected at an angle, unbalancing the quadrant detector.

1.6.1 Estimation of expected amplitude

In order to get an estimate of the deflection the light beam experiences due to the oscillation of a resonator, the modeshape function of a resonator can be inspected. Based on the shape and a given displacement amplitude the approximate displacement can be calculated to get an idea of the obtained signal. The starting point is the mode shape of a rectangular membrane $\phi_{n,j}(x,y)$ [15]:

$$\phi_{n,j}(x,y) = \sin\left(\frac{n\pi x}{L_x}\right)\sin\left(\frac{j\pi y}{L_y}\right) \tag{1.11}$$

Where n and j represent the mode numbers, that combined identify the individual resonance modes. L_x and L_y are the lengths in the respective dimension. This mode shape is the displacement of the resonator and in this formula it is normalized to 1. For a real resonator, the amplitude has to be adjusted. The amplitude can be obtained via measurements with an LDV or for a theoretical approach, the critical amplitude z_c before the onset of nonlinearity can be used.

$$z_c = \sqrt{\frac{8}{3\sqrt{3}}}\frac{1}{\sqrt{Q}}\sqrt{\frac{m\omega_0^2}{\alpha}} \tag{1.12}$$

Die approbierte gedruckte Originalversion dieser Diplomarbeit ist an der TU Wien Bibliothek verfügbar
The approved original version of this thesis is available in print at TU Wien Bibliothek.

Where z_c is the critical amplitude, Q the quality factor of the resonator, m the effective mass, ω_0 the resonance frequency and α the duffing parameter [15].
The maximum displacement amplitude A_0 is applied to Equation (1.11) and the mode shape function scales accordingly (equ. (1.13)).

$$A_{n,j}(x,y) = A_0 \sin\left(\frac{n\pi x}{L_x}\right) \sin\left(\frac{j\pi x}{L_y}\right) \tag{1.13}$$

The optical lever technique relies on changes in angle rather than changes in displacement. Therefore, the first derivative, which represents the change in displacement, is of interest rather than the mode shape, since the mode shape depends on two variables, the total derivative has to be calculated as is shown in Equations (1.14), (1.15) and (1.16):

$$dA_{n,j}(x,y) = \frac{dA_{n,j}(x,y)}{dx} + \frac{dA_{n,j}(x,y)}{dy} \tag{1.14}$$

The derivative for each dimension being as follows:

$$\frac{dA_{n,j}(x,y)}{dx} = A_0 \frac{n\pi}{L_x} \cos\left(\frac{n\pi x}{L_x}\right) \sin\left(\frac{j\pi y}{L_y}\right) \tag{1.15}$$

$$\frac{dA_{n,j}(x,y)}{dy} = A_0 \frac{j\pi}{L_y} \sin\left(\frac{n\pi x}{L_x}\right) \cos\left(\frac{j\pi y}{L_y}\right) \tag{1.16}$$

Together, they describe the angle across the surface of the membrane as described in Equation (1.17).

$$\begin{aligned} dA_{n,j}(x,y) = A_0 \Bigg(& \frac{n\pi}{L_x} \cos\left(\frac{n\pi x}{L_x}\right) \sin\left(\frac{j\pi y}{L_y}\right) \\ & + \frac{j\pi}{L_y} \sin\left(\frac{n\pi x}{L_x}\right) \cos\left(\frac{j\pi y}{L_y}\right) \Bigg) \end{aligned} \tag{1.17}$$

Since the two terms are identical, just originating from a different dimension, for harmonic ($n = j$) modeshapes of a square membranes ($L_x = L_y$) the equation reduces to Equation (1.18).

Die approbierte gedruckte Originalversion dieser Diplomarbeit ist an der TU Wien Bibliothek verfügbar
The approved original version of this thesis is available in print at TU Wien Bibliothek.
TU Bibliothek Your knowledge hub WIEN

$$\frac{dA_n(x)}{dx} = A_0 \frac{n\pi}{L_x} \cos\left(\frac{n\pi x}{L_x}\right) \tag{1.18}$$

The cosine part of the equation can be solved for $max(\cos\left(\frac{n\pi x}{L_x}\right)) = 1$, since the focus is on the maximum values.

$$\frac{dA_n(x)_{\max}}{dx} = A_0 \frac{n\pi}{L_x} \tag{1.19}$$

These maxima occur physically for different modes in different positions of x. These positions at multiples of $x = \frac{L_x}{n}$ (for $0 < x < L_x$) are the nodal points of the mode shape, where the amplitude is at its minimum and the angle at its maximum.

With a known displacement A_0, the change in angle and therefore the change in displacement on the detector can be estimated. For a square membrane of $L_x = L_y = L = 1$ mm and an amplitude of $A_0 = 10$ nm, the maximum angle in one dimension comes out to (1.20).

$$\alpha_{\max} = \frac{dA_{\max}(n)}{dx} = A_0 \frac{n\pi}{L_x} = 10^{-6} n\pi \tag{1.20}$$

This change in angle is then leveraged through the optical path to enhance the displacement on the detector. The longer the optical path, the greater the effect. To determine the actual displacement on the detector d, Equation (1.21) shows the trigonometric relationship that is equivalent to this enhancement:

$$d = \tan(\alpha_{max}) f_{\text{focal}} = \tan\left(A_0 \frac{n\pi}{L_x}\right) f_{\text{focal}} \tag{1.21}$$

In this work the laser spot is focused on the resonator; therefore, the length of the optical lever is given by f_{focal} which is the focal length of the lens. For a lens with a focal length of $f_{\text{focal}} = 125$ mm, an estimate of the displacement of the reflected beam spot for the first resonance mode ($n = 1$) can be made (equ. (1.22)).

$$d = \tan\left(\pi \frac{10^{-8}}{10^{-3}}\right) \cdot 125 \cdot 10^{-3} \approx 4\mu m \tag{1.22}$$

Die approbierte gedruckte Originalversion dieser Diplomarbeit ist an der TU Wien Bibliothek verfügbar
The approved original version of this thesis is available in print at TU Wien Bibliothek.
TU Bibliothek Your knowledge hub WIEN

Figure 1.8 shows the linear relation between deflection of the reflected beam on the detector and the mode number for a fixed oscillation amplitude. The deflection on the detector only depends on the focal length since after the reflected beam passes the lens again, it is collimated.

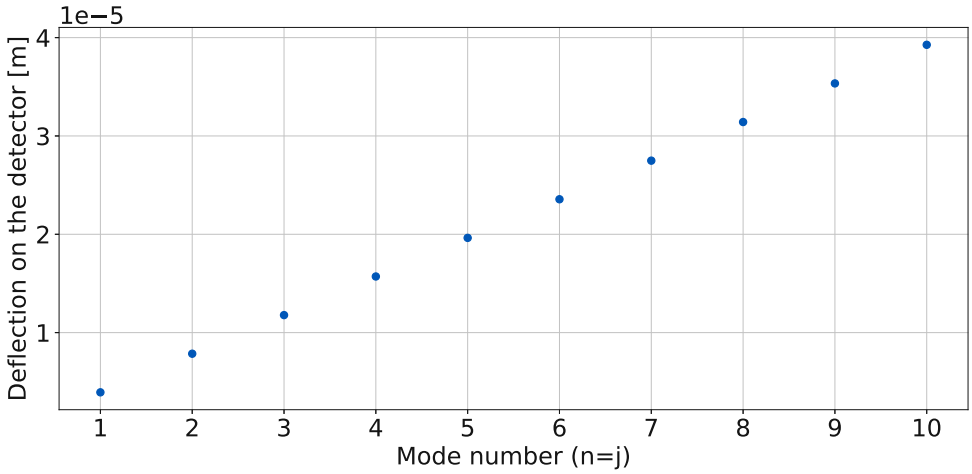

Figure 1.8: Deflection d of the light beam on the detector after an optical lever of 125 mm for increasing mode numbers

The expected displacement for a resonator driven at its critical amplitude is approximately 4 µm. However, given a sufficiently high Q-factor, even an undriven resonator exhibits a measurable displacement.
Using the same membrane as above, and assuming a quality factor Q, effective mass m_{eff}, angular resonance frequency ω_0, and temperature T together with the Bolzmann constant k_B, the mean square of the thermomechanical displacement, $\langle z_{th}^2 \rangle$, can be estimated according to [15] (equ. (1.23)).

$$\langle z_{th}^2 \rangle = \frac{k_B T}{m_{eff} \omega_0^2} \tag{1.23}$$

Then the Root-Mean-Square of the displacement, z_{RMS} is given by Equation (1.24), which is the effektive displacement of the resonator due to thermo-

Die approbierte gedruckte Originalversion dieser Diplomarbeit ist an der TU Wien Bibliothek verfügbar
The approved original version of this thesis is available in print at TU Wien Bibliothek.

mechanical noise.

$$z_{RMS} = \sqrt{\langle z_{th}^2 \rangle} = \sqrt{\frac{k_B T}{m_{eff}\omega_0^2}} \tag{1.24}$$

The effective mass m_{eff} originates from the design of the resonator and its material. For a square membranes the effective mass is given by Equation (1.25) [15]:

$$m_{eff} = \frac{m_0}{4} \tag{1.25}$$

m_0 is the actual mass of the resonator and in this case, which can be easily calculated using the density of silicon nitride ρ, its thickness h and its side length L. The factor of $\frac{1}{4}$ is due to the design of the resonator [15].

$$m_0 = L^2 h \rho \tag{1.26}$$

The density of silicon nitride, ρ, was taken from the literature [22], while the other parameters were approximated from previous measurements. The quality factor Q can either be estimated theoretically or measured experimentally. A ring-down measurement or the measurement of the Full-Width at Half-Maximum (FWHM) of a resonance allows for the determination of Q. For high-Q resonators, the ring-down method is preferred since the resonator linewidth decreases with increasing Q [15, 23, 24].

Parameter	Value	Unit
L	1000	μm
h	50	nm
ρ	3000	kg/m^3
m_{eff}	37.5×10^{-12}	kg
Q	10^5	-
ω_0	150·2π	rad/s
T	300	K

Table 1.1: Parameters used for the estimation of the critical amplitude.

Given the parameters in 1.1 and Equation (1.23) the RMS of the thermome-

Die approbierte gedruckte Originalversion dieser Diplomarbeit ist an der TU Wien Bibliothek verfügbar
The approved original version of this thesis is available in print at TU Wien Bibliothek.

chanical displacement can be calculated as shown in Equation (1.27)

$$z_{RMS} \approx 1.1 \times 10^{-11}\,\mathrm{m} \tag{1.27}$$

And finally, the displacement on the detector due to the thermomechanical noise of the first resonance mode can be estimated using Equation (1.21).

$$d = \tan\left(\pi \frac{z_{RMS}}{L}\right) f_{\mathrm{focal}} \approx 4.38\,\mathrm{nm} \tag{1.28}$$

Equation (1.28) indicates that for the thermomechanical noise peak of the fundamental mode of a 1 mm square membrane, the expected displacement on the detector is approximately 4.38 nm.

Die approbierte gedruckte Originalversion dieser Diplomarbeit ist an der TU Wien Bibliothek verfügbar
The approved original version of this thesis is available in print at TU Wien Bibliothek.
TU Bibliothek Your knowledge hub WIEN

1.7 Laser Doppler Vibrometer

A laser Doppler vibrometer is an advanced optical measurement tool used in various fields, including NEMS, for non-contact and highly sensitive measurement of vibrations and displacements. It is a versatile instrument that can provide precise measurements of dynamic behavior.

The LDV operates based on the Doppler effect, which is the shift in frequency of a wave (such as light) when observed from a moving source due to velocity. In the context of an LDV, the source is a laser beam, and the observed object is the vibrating structure. The LDV emits a laser beam towards the surface of the NEMS and it is partially reflected by the surface. Because of the velocity of the vibrating surface, the reflected light experiences a small shift in frequency due to the Doppler effect. By splitting the laser beam into two paths at the source, one independent reference beam and one signal beam can be kept separate. The signal beam reaches the object of interest and has its frequency shifted, while the reference beam is kept internal and experiences no outside influence. By interfering the two beams, due to the difference in frequency, information about the velocity can be inferred [25, 26].

In the context of NEMS and MEMS, LDVs are used for various purposes, such as measuring the resonant frequencies, vibrational modes, and damping characteristics of such devices. LDVs are especially valuable when working with delicate or complex resonators where contact-based measurements might disturb the behavior being studied.

Die approbierte gedruckte Originalversion dieser Diplomarbeit ist an der TU Wien Bibliothek verfügbar
The approved original version of this thesis is available in print at TU Wien Bibliothek.

1.8 Fourier-Transform-Infrared-Spectroscopy

One of the applications of tracking the resonance frequency of NEMS lies in spectroscopy [27–30], particularly in infrared spectroscopy. One application of this is combining NEMS with a Fourier-Transform Infrared Spectroscopy (FTIR) device and depositing an analyte onto the NEMS structure, directing the light from FTIR device onto the resonator and recording its reaction in frequency to the incident light. FTIR is a powerful analytical technique that employs the mathematical principles of Fourier transformation to analyze the interaction of light with a sample, converting signals from the time domain to the frequency domain. This process results in a spectrum of frequencies that correspond to the unique vibrational modes of the molecules that make up the sample.

The key component of an FTIR system is the Michelson interferometer, which modulates a broadband infrared light source by splitting it into two beams that travel different optical paths before recombination. As the movable mirror shifts, the recombined beams undergo constructive and destructive interference at different optical path differences, leading to a varying intensity pattern known as an interferogram. This interferogram contains contributions from all wavelengths of the light source simultaneously. When this beam illuminates the sample placed between the light source and photodetector, specific molecular vibrations within the sample absorb light at characteristic wavelengths. This absorption causes the transmitted light after the sample to have a reduced intensity for these wavelengths. By tracking the transmitted light and processing them with the FTIR system, the absorption characteristics of the sample can be obtained.

The data acquired in the time domain is then transformed into a frequency spectrum using a Fast Fourier Transform (FFT). The resulting spectrum reveals the absorption profile of the sample as a function of the wavenumber or wavelength.

The spectrum produced by FTIR serves as a molecular fingerprint of the an-

Die approbierte gedruckte Originalversion dieser Diplomarbeit ist an der TU Wien Bibliothek verfügbar
The approved original version of this thesis is available in print at TU Wien Bibliothek.
TU Bibliothek Your knowledge hub WIEN

alyte, with each peak and valley corresponding to distinct molecular bonds and structures. This capability enables the identification and characterization of the chemical composition of a sample. Additionally, FTIR offers significant advantages over dispersive spectroscopic methods. One of its most notable features is speed: FTIR can capture information across all wavelengths simultaneously, making it an exceptionally fast and efficient tool for molecular analysis. This efficiency, combined with its ability to provide detailed molecular information, makes FTIR a cornerstone technique in fields ranging from materials science to biochemistry [31].

Die approbierte gedruckte Originalversion dieser Diplomarbeit ist an der TU Wien Bibliothek verfügbar
The approved original version of this thesis is available in print at TU Wien Bibliothek.

Chapter 2

Methods

Die approbierte gedruckte Originalversion dieser Diplomarbeit ist an der TU Wien Bibliothek verfügbar
The approved original version of this thesis is available in print at TU Wien Bibliothek.

2.1 NEMS Resonator

Nano-Electro-Mechanical System resonators exist in a range of variations, defined by their shape and the physical properties of the materials from which they are made. The resonators used in this work are low-pressure chemical vapor deposition (LPCVD) silicon nitride (SiN) square membranes with a perforated central area. The membrane measures 1 mm per side and has a thickness of 50 nm.

The wafer from which the resonator chips are fabricated consists of three layers: a 380 µm thick silicon (Si) layer, with thin SiN layers on both the top and bottom. The top SiN layer later forms the membrane, but to create a free-standing membrane, the bulk Si underneath must be removed.

The membrane resonators used in this work feature an array of perforations in their central region, with a total diameter of approximately 600 µm. The perforations consist of 6 µm large holes and a distance of 3 µm between the holes. Originally designed for spectroscopy [29], these perforations allow targeted particle deposition in the center. As demonstrated by Luhmann et al. [29], the resonator can be used in combination with a light source for infrared spectroscopy.

The fabrication process is briefly illustrated in Figure 2.1. The patterning of the individual layers was performed using photolithography, with masks containing the designs for each fabrication step across the entire wafer.

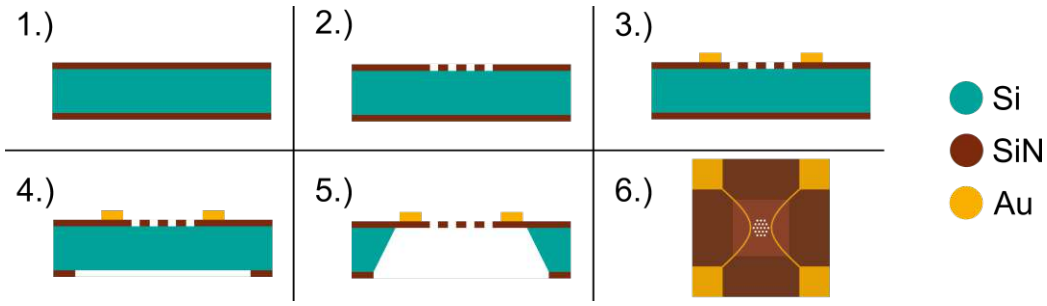

Figure 2.1: Steps of the fabrication process

The first step (1) shows the clean wafer as received from the manufacturer,

Die approbierte gedruckte Originalversion dieser Diplomarbeit ist an der TU Wien Bibliothek verfügbar
The approved original version of this thesis is available in print at TU Wien Bibliothek.

consisting of a silicon layer sandwiched between two silicon nitride layers. As the first fabrication step (2), perforations are etched into the SiN using reactive-ion etching (RIE). Next (3), two electrodes are added by depositing a thin layer of chromium (5 nm) followed by a gold layer (95 nm) via physical vapor deposition (PVD). The chromium layer, though not depicted, enhances adhesion between the gold and SiN.

The final processing step involves removing the bulk silicon to release the membrane, allowing it to oscillate freely. This is done by partially etching the backside SiN via RIE (4), followed by potassium hydroxide (KOH) etching, which selectively removes silicon while leaving SiN nearly unaffected. Only previously exposed areas are etched, while the rest remains intact (5). Finally, the completed wafer is dried and broken into individual chips, each featuring a central membrane with perforations and electrodes on top (6).

For magnetomotive read-out, electrodes are required. However, for optical read-out, they are unnecessary. Since the gold layer affects the characteristics of the resonator, the electrode deposition step (3) was omitted for the resonators used in the optical system comparison. The resonators used in this work have been fabricated in a local clean room, but their fabrication is outside the scope of this work.

The resonators in this work are operated in a vacuum environment to reduce the effect of damping and thermal conductivity caused by the presents of gas [15]. The pressure for for all measurements is reduced to at least 1×10^{-5} mbar.

Die approbierte gedruckte Originalversion dieser Diplomarbeit ist an der TU Wien Bibliothek verfügbar
The approved original version of this thesis is available in print at TU Wien Bibliothek.

2.2 Optical Lever Setup

In this work the optical lever is implemented with a single optical arm and a beamsplitter, which means that the incoming and reflected light pass through mostly the same optical components. A more common implementation uses two separate paths; one for the incoming beam and then another independent one for the reflected beam. By using a single optical path for most of the light, misalignment issues and differences in the paths are reduced. Since the same path is used for the incoming and reflected light beam, there is a need to distinguish between the two. A very compact and straightforward way of achieving this is a polarizing beamsplitter combined with a quarter waveplate, as was demonstrated by [32].

The main components used in this work are described below and Figure 2.2 shows the configuration of optical components and the resonator setup.

The laser diode (Thorlabs laser module LDM785) produces a collimated, elliptical beam with a wavelength of 785 nm. A pinhole then reshapes the beam into a smaller, circular profile. This reshaped beam enters a polarizing beamsplitter (CCM1-PBS252/M), which is precisely aligned to the polarization of the laser beam to ensure maximum transmission. After passing through the beamsplitter, the beam encounters a zero-order waveplate (WPQ05M-780), which rotates the polarization of the transmitted light by 45°. The light then encounters the target from which it reflects and passes through the waveplate again. The light undergoes an additional 45° polarization shift, resulting in a total change of 90° with respect to the original beam. Due to this polarization shift, the beamsplitter redirects the light to an orthogonal output instead of back to the laser. At this output, a photodetector (QP5.8-6 TO) is placed to capture and analyze the reflected light. In order to remove the impact of light, which is not of the wavenumber of the laser, a wavelength band pass was installed right before the detector (Thorlabs FBH790-10).

Die approbierte gedruckte Originalversion dieser Diplomarbeit ist an der TU Wien Bibliothek verfügbar
The approved original version of this thesis is available in print at TU Wien Bibliothek.
TU Bibliothek Your knowledge hub WIEN

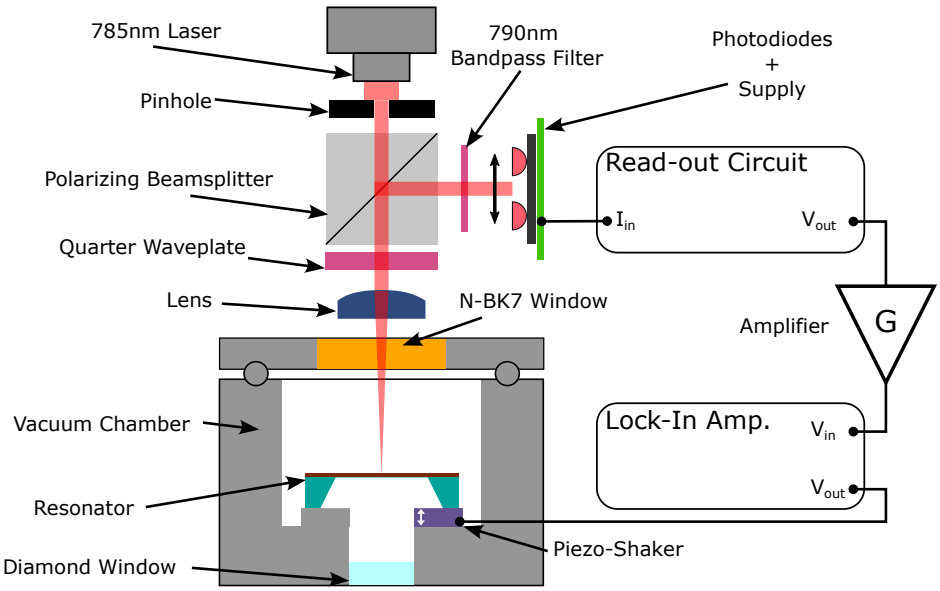

Figure 2.2: Measurement setup for the optical lever readout.

Laser Diode: The laser diode provides coherent, monochromatic light through stimulated emission. By stimulating photon emission in a p-n junction and amplifying it within an optical cavity. Important for this application is the collimated and coherent output of the laser.

Pinhole: The laser beam shape provided by the laser diode is rather large and elliptic with a shape of roughly 2.6 mm x 4.4 mm. Therefore, a pinhole is placed right after the diode to restrict the shape to a smaller circular shape. It was set to a hole with a diameter of 0.5 mm.

Polarizing Beamsplitter: Polarizing beamsplitters operate on the principle of polarization-based separation of an incident light beam. Utilizing materials with birefringent properties, and a thin film coating, the beamsplitter effectively separates the s-polarized and p-polarized components. While one component passes through the beamsplitter unimpeded, the other component is reflected at a 90° angle. This creates two separate beam paths, with one component of the light each. In this work the beamsplitter is aligned so all the incoming light from the laser, is transmitted to the resonator. The

Die approbierte gedruckte Originalversion dieser Diplomarbeit ist an der TU Wien Bibliothek verfügbar
The approved original version of this thesis is available in print at TU Wien Bibliothek.

reflected light has a change of polarity due to the waveplate and therefore is reflected at a 90° angle, effectively separating the incoming laser light from the reflected light. The reflected light contains information regarding the resonator; therefore, the detector is placed on this side of the beamsplitter.

Zero Order Quarter Waveplate: The $\frac{\lambda}{4}$ waveplate introduces a phase shift, effectively causing a 45° rotation in the polarization of linearly polarized light. This phase alteration transforms the light into an elliptically polarized form. This property is used to distinguish between the incoming and reflected beams. The incoming light passes through the waveplate, and by being reflected off of a surface, it causes the elliptical polarization to change direction. Passing through the $\frac{\lambda}{4}$ waveplate a second time, results in singular polarized light with a 90° phase change in total, compared to the original incoming light.
The principle of optical separation using a quarter waveplate and a polarizing beamsplitter is well illustrated by Edmund optics [33].

Detector: Photodiodes convert light into electrical current via the photovoltaic effect. Photons incident on the diode generate electron-hole pairs, creating a photocurrent. In particular, quadrant photodetectors, with their quadrant-based structure, excel in determining the position of incident light. By combining the photocurrent of all 4 quadrants information about the position can be determined. More on this in section 2.2.1.

Lens: The plano-convex lens, with a flat and a convex surface focuses and collimates light depending of the orientation. In the setup used in this work, the lens first focuses the incoming light onto the NEMS device and then re-collimates the reflected light. Because the optical lever depends on the distance the uncollimated light travels after being reflected, a longer focus length of the lens leads to a larger displacement on the detector, but no matter what, light will eventually diverge, which reduces the effectiveness of the optical lever.

Die approbierte gedruckte Originalversion dieser Diplomarbeit ist an der TU Wien Bibliothek verfügbar
The approved original version of this thesis is available in print at TU Wien Bibliothek.
TU Bibliothek Your knowledge hub WIEN

Optical Port: The optical port allows light to pass to the insides of the vacuum chamber without impacting the vacuum itself. The most important requirement for this component is that it is highly transmissible for the wavelength of the light used. N-BK7 is a material that is highly transmissible in the wavelength range of 350 nm - 2 µm. The optical window in this work has a specific coating for wavelengths between 650 nm - 1050 nm$650nm - 1050nm$ (Thorlabs WG11050-B), which allows the wavelength of the laser to pass, but blocks out a large part of the light spectrum that is of no interest.

The setup regarding the resonator consists of a vacuum chamber connected to a vacuum pump system (Agilent TPS-mini) and a piezo shaker below the resonator for actuation. The read-out uses the optical lever setup with the laser beam being positioned on the resonator through the optical port. The optical lever setup implements the technique as described above and the generated photocurrents are converted to a voltage signal as described in section 2.2.1. The generated oscillation is then further amplified using a low noise voltage amplifier (SR560 Stanford Research Systems). A lock-in amplifier (Zurich Instruments MFLI) is fed the amplified signal, where a PLL locks onto the resonance frequency and keeps track of it while providing the drive for the piezo shaker. The optical assembly itself is fixed on top of an XY-stage that is itself mounted to the vacuum chamber. This allows for the positioning of the beam spot to different locations on the resonator without changing the optical arm itself.
The proper measurement procedure includes the tuning of the laser power, which was simply done by adjusting the potentiometer screw on the laser module. In order to be certain about the light power though, an external photodetector (Thorlabs S120VC) was used to measure the power of the laser light after the optical port and at approximately the same distance to the detector as the resonator is positioned. This is to make sure, which power reaches the resonator in every case and measurement.

Die approbierte gedruckte Originalversion dieser Diplomarbeit ist an der TU Wien Bibliothek verfügbar
The approved original version of this thesis is available in print at TU Wien Bibliothek.
TU Bibliothek Your knowledge hub WIEN

2.2.1 Photodiode Circuit

The optical lever technique uses optical elements to create a beam of light whose center is displaced depending on the angle of the reflecting surface. To accurately track the position of this reflected beam, this work utilizes a quadrant photodiode. Each quadrant contains an identical photodiode, which generates a current in response to incident light and is separated by only a small gap of 24 µm (fig. 2.4 shows a schematic). There are two ways to use this current: either the currents are directly processed or the current is converted to a voltage. For voltage signals a transimpedance amplifier (TIA) circuit can be implemented, which converts and amplifies these minute currents into voltage signals that can then be further analyzed with appropriate instruments. While it can be beneficial to process the signals as current and then convert the final signal to voltage, this approach comes with a more complicated design that requires fine-tuning of every component [34]. Especially the tuning of the bias currents of each transistor makes the design complicated and hard to scale. This work considered implementing the current-based approach but ultimately opted for the voltage-based implementation due to its simplicity and ease of use.

The transimpedance amplifier operates via an operational amplifier (op-amp) in conjunction with a feedback resistor (R_f) and a few capacitors. The resistor determines the gain of the TIA, dictating the conversion ratio between input current and output voltage. The TIA used here is displayed in Figure 2.3. To enhance the stability of the amplifier, a parallel feedback capacitor, C_f, is installed alongside the feedback resistor R_F. This capacitor plays a vital role in managing the frequency response and maintaining the phase margin of the amplifier, mitigating potential oscillations and ensuring reliable operation [35].

Die approbierte gedruckte Originalversion dieser Diplomarbeit ist an der TU Wien Bibliothek verfügbar
The approved original version of this thesis is available in print at TU Wien Bibliothek.

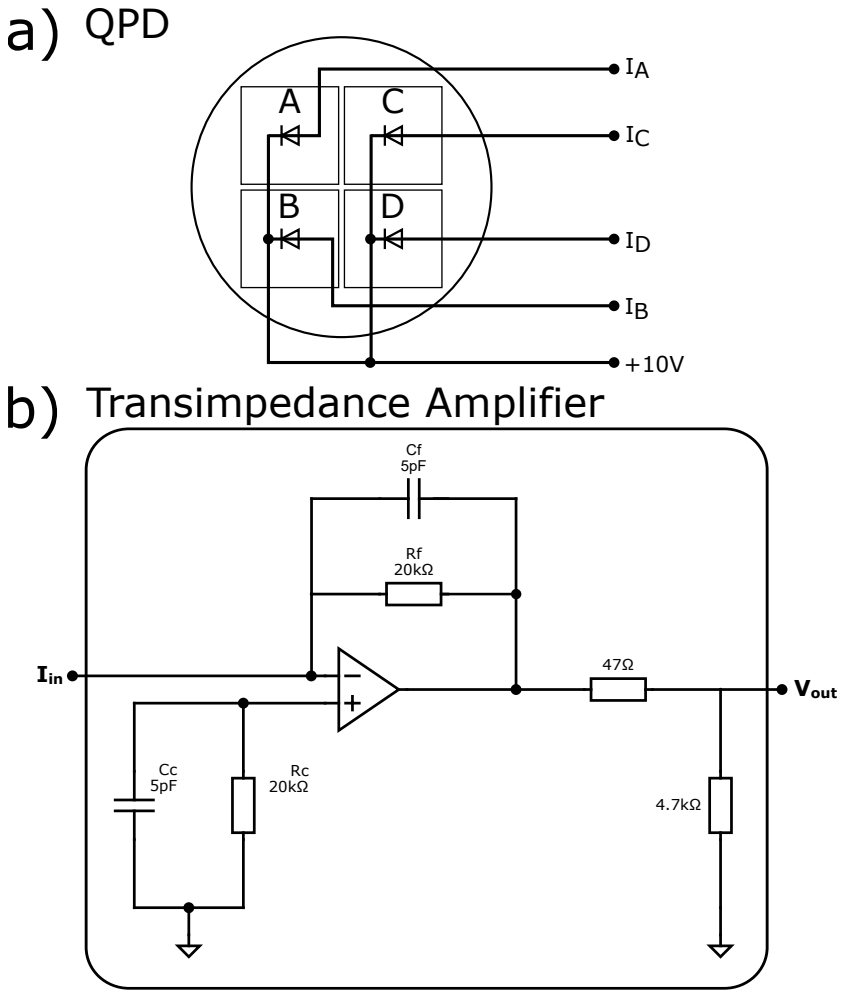

Figure 2.3: a) Electric schematic of photodiodes in parallel generating a photocurrent based on the respective light exposure each. b) Transimpedance amplifier circuit implementation that transforms the incoming diode current into a voltage signal.

Each quadrant of the split photodiode is connected to one transimpedance amplifier, which converts each respective diode current into a voltage. Depending on the orientation of the deflection on the detector, the configuration for measuring oscillations may vary. When the beam is situated at the boundary of one quadrant and the oscillation moves out of its bounds, the photocurrent of this quadrant follows an oscillating signal. However, if the beam is positioned between two photodiodes, resulting in two signals that

Die approbierte gedruckte Originalversion dieser Diplomarbeit ist an der TU Wien Bibliothek verfügbar
The approved original version of this thesis is available in print at TU Wien Bibliothek.

are 180° phase-shifted, feeding these signals into a differential amplifier effectively doubles the amplitude of the oscillating signal while removing common noise. This concept is depicted in Figure 2.4, where the beam spot moves between quadrant A and D, generating an oscillation. Subtracting these signals produces a new signal with the the same frequency, but double the amplitude.

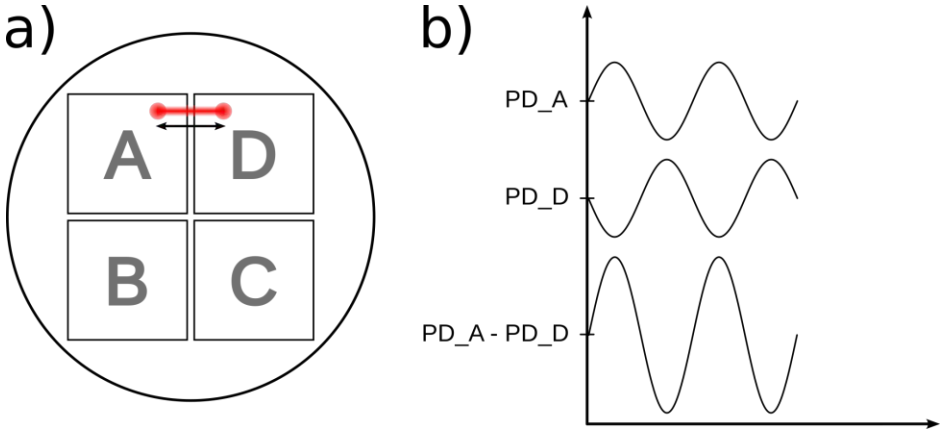

Figure 2.4: a) Schematic of the quadrant photodetector with the beam spot moving between quadrant A and D. b) Corresponding signals generated from photodiodes A and B and their difference.

The utilization of four quadrants provides flexibility for measurements in two dimensions. Depending on the resonance mode of the NEMS and the placement of the laser beam on the resonator, the movement of the reflected beam varies. If only two diodes are used, the beam on the detector may move either horizontally or vertically. Depending on the photodiodes used for the read-out, oscillations might not be detected at all.
If necessary, there is the option to calculate two separate signals, essentially the X and Y components of the deflection on the detector. In Figure 2.4 only an oscillation along the X-Axis is assumed. However, considering there could be a diagonal displacement of the beam, some information about the movement would be lost.
To capture the total deflection, the two signals

$$X = PD\_D + PD\_A - (PD\_B + PD\_C) \tag{2.1}$$

Die approbierte gedruckte Originalversion dieser Diplomarbeit ist an der TU Wien Bibliothek verfügbar
The approved original version of this thesis is available in print at TU Wien Bibliothek.

$$Y = PD\_A + PD\_D - (PD\_B + PD\_C) \tag{2.2}$$

are computed via an additional subtracting operational amplifier circuit. To determine the total length, which can now be considered the magnitude of a vector

$$\vec{S} = \begin{pmatrix} X \\ Y \end{pmatrix} \tag{2.3}$$

the quadrature must be formed:

$$|\vec{S}| = \sqrt{X^2 + Y^2} \tag{2.4}$$

This may be a simple operation in a mathematical context, but in electrical circuits it is quite complicated to implement. One way to accomplish this is by using a micro-controller or FPGA to convert the voltages to digital values, perform these additional operations, and then convert the results back into analog signals. For the sake of simplicity, this work focuses on either the X or Y component and therefore, only uses two photodiodes at a time.

2.2.2 Measurement Procedure

The standard procedure for each measurement is to place the resonator in the vacuum chamber on top of the piezo shaker. The vacuum chamber is closed, the vacuum pump started, the optical components installed on top of it and then some time has to pass until the vacuum reaches a stable pressure of 1×10^{-5} mbar. Then the laser is turned on while the output voltages of two out of the four quadrants of the photodiode are observed. The laser is positioned on the resonator via the XY-stage of the optical arm. The photodiode has its own translation stage to adjust the alignment of the reflected beam and the detector. The alignment of the reflected beam to the photodiode is adjusted until the voltages of the two diodes show the same absolute DC voltage. At this point the membrane does not oscillate yet, but rather acts as a reflective surface. Once the signals are balanced, an appropriate frequency range is chosen for which the lock-in amplifier performs a frequency sweep. If correctly aligned, the sweep shows one or more resonance peaks similar to

Die approbierte gedruckte Originalversion dieser Diplomarbeit ist an der TU Wien Bibliothek verfügbar
The approved original version of this thesis is available in print at TU Wien Bibliothek.

1.3. In case this is not observed, the alignment of the optical setup to the resonator or the alignment of the reflected beam to the photodiode has to be adjusted. Depending on the resonance mode, the reflected beam is displaced in a certain direction on the detector, and this direction of displacement has to match the two photodiodes connected to the lock-in amplifier. Once the desired resonance frequency is found, it can be locked using a PLL and the oscillation amplitude can be plotted and observed. The laser has up to this moment only been roughly aligned to the resonator, but now that the resonance is locked, the alignment can be fine-tuned by observing the voltage amplitude while moving the laser spot.

By moving along one axis at a time, the modeshape can also be observed since the amplitude shows its maximum when the laser is positioned on the nodal points and the minimum at the anti-nodal points. One such measurement is shown in Figure 2.5(d), where the laser beam spot was positioned at the center of the membrane along the Y-axis and slightly off the membrane along the X-axis. By gradually moving the laser across the membrane in the X-axis while maintaining its Y position, changes in amplitude were observed. The amplitude reaches a maximum at the center of the membrane, with two local maxima closer to the rim. This pattern aligns well with the expected mode shape, including its nodal and anti-nodal points as can be seen with the comparison in Figure 2.5(d). The increased amplitude at the center, compared to positions near the edges, is attributed to the size of the beam spot. The distorted shape is due to the imprecision of moving the laser with a manual XY-stage which was simply translated by hand. This behavior can also be calculated using the theoretical mode shapes shown in section 1.2 based on equations established in [15]. The results of this calculation is shown in Figure 2.5(a-d).The derivative of the mode shape represents the change in angle and a Gaussian distribution is chosen to represent the laser beam. The convolution of the derivative and the Gaussian distribution of the laser show a very similar result as the measurement as can be seen in Figure 2.5(d).

Die approbierte gedruckte Originalversion dieser Diplomarbeit ist an der TU Wien Bibliothek verfügbar
The approved original version of this thesis is available in print at TU Wien Bibliothek.
TU Bibliothek Your knowledge hub WIEN

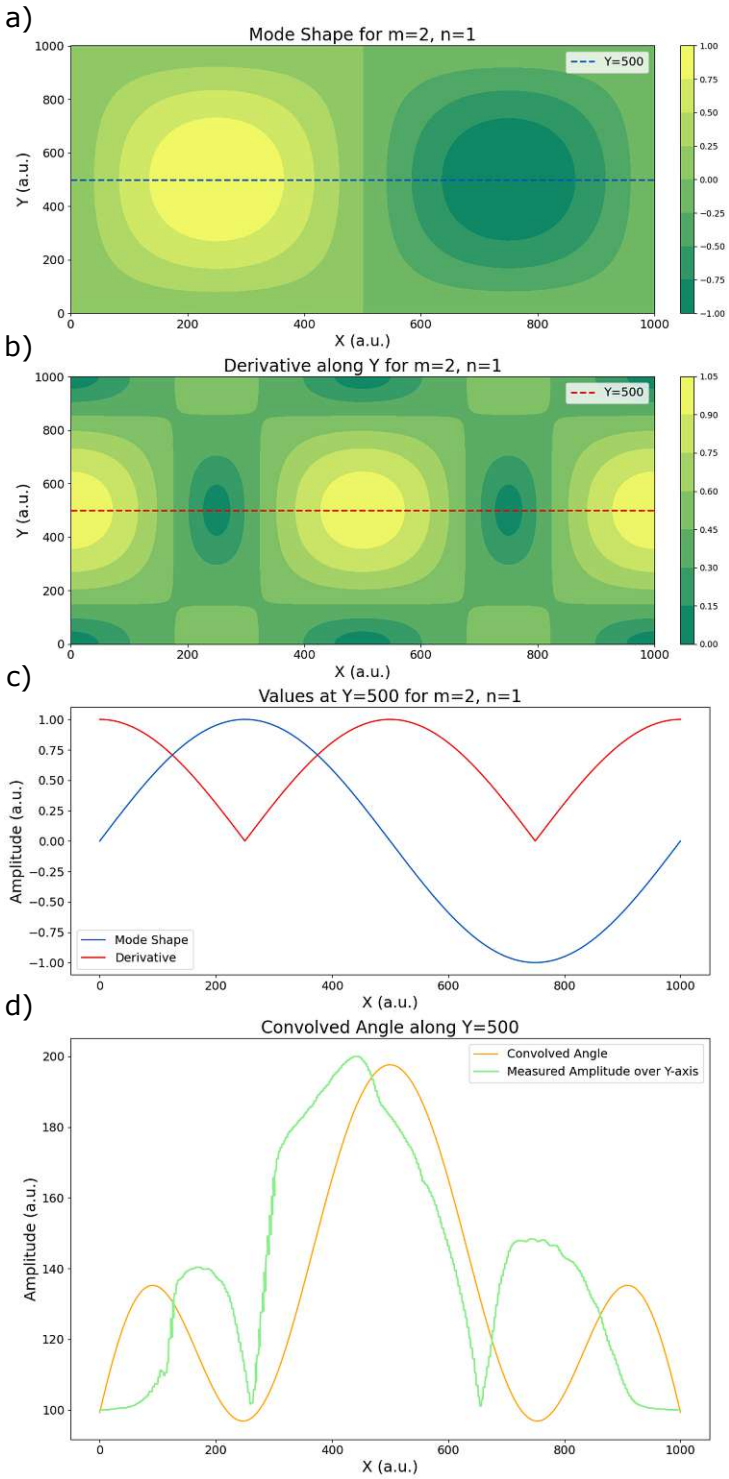

Figure 2.5: a) shows the simulated mode shape of a membrane for the "1,2" mode. b) is the derivative of this modeshape along the Y-axis. c) shows the modeshape and derivative along the center of the Y-axis. d) shows the convolved signal of a Gaussian beam, with a diameter of 220 µm and the derivative of the modeshape in the center of the X-axis.

Die approbierte gedruckte Originalversion dieser Diplomarbeit ist an der TU Wien Bibliothek verfügbar
The approved original version of this thesis is available in print at TU Wien Bibliothek.

For this work the resonance mode "1,2" is used for all measurements, since this one also works particularly well for the magnetomotive read-out.

Once optimized, the first step is to characterize the resonator with a ring down measurement and by measuring the thermomechanical noise peak using the spectral analyzer of the lock-in amplifier. Using these measurements, the critical amplitude can then be calculated (see section 1.6.1) and the drive adjusted to match this amplitude in voltage (see section 1.3). Once this is established, the frequency stability measurement can be measured for 1 minute.

2.3 Magnetomotive Technique Setup

The magnetomotive readout employs an electrical principle in which a magnetic field induces currents in an electrode placed on the resonator. These currents provide a readout of the oscillation amplitude of the resonator [3, 15, 29, 36]. Unlike the optical lever technique, no additional actuation mechanism is necessary because one electrode can serve as read-out and one for actuation. A lock-in amplifier(Zurich Instruments MFLI) is used to process the signal, and its PLL is employed for tracking the resonance frequency changes. Figure 2.6 depicts the magnetomotive readout setup. Including a set of magnets, an amplifying circuit and the lock-in amplifier.

Die approbierte gedruckte Originalversion dieser Diplomarbeit ist an der TU Wien Bibliothek verfügbar
The approved original version of this thesis is available in print at TU Wien Bibliothek.

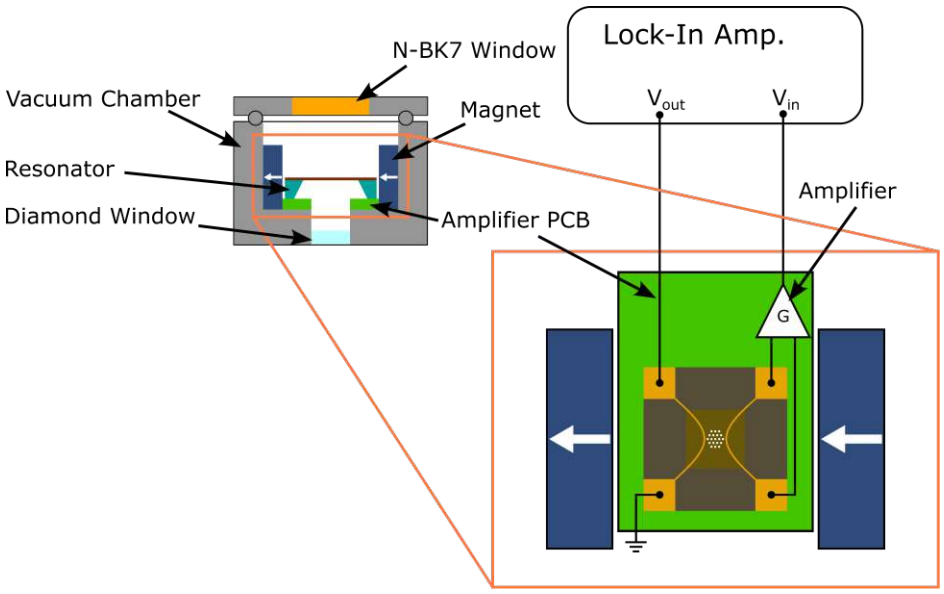

Figure 2.6: Measurement setup for the magnetomotive readout.

2.3.1 Measurement Procedure

Since the magnetomotive read-out is not sensitive enough to resolve the thermomechanical noise peak and does not require optical alignment, the measurement procedure is relatively simple. The chip is installed, the electronic connection to the electrodes is established, and the vacuum system is started. Once the system reaches a pressure of 1×10^{-5} mbar, measurements can begin. The resonance is then searched for via a frequency sweep and locked. The amplitude of the drive is estimated by observing the locked frequency of the resonator and adjusted until there is no observable jump in frequency. Then the frequency stability is recorded for 1 minute.

2.4 Laser Doppler Vibrometer Technique Setup

The laser Doppler Vibrometer is a widely recognized optical method for displacement and velocity measurements. In this study, the LDV setup uses a

Die approbierte gedruckte Originalversion dieser Diplomarbeit ist an der TU Wien Bibliothek verfügbar
The approved original version of this thesis is available in print at TU Wien Bibliothek.

vacuum chamber different from the one used for the optical lever and magnetomotive setups due to the shorter focal length of the particular LDV configuration used in this work. The laser power was measured with an external power meter (Thorlabs S120VC) after the window, to guarantee the power reaching the resonator is known.
The LDV (Polytec MSA-500) measures the velocity of the resonator surface via the Doppler effect while a piezo actuator provides the driving force for the resonator. A lock-in amplifier(Zurich Instruments MFLI) and PLL process and track the frequency of the resonator. Figure 2.7 illustrates the LDV measurement setup.

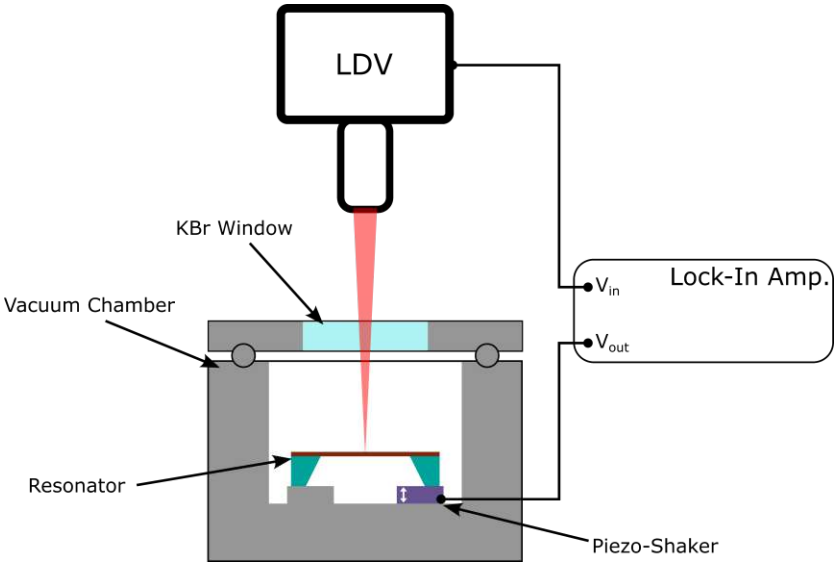

Figure 2.7: Measurement setup for the laser Doppler Vibrometer readout.

2.4.1 Measurement Procedure

The laser Doppler Vibrometer, similar to the optical lever technique requires the calibration of the system to drive the resonator at the appropriate displacement amplitude, so the first steps are the ring down measurement and thermomechanical noise measurement. For this the resonator has to be placed in the vacuum chamber and the vacuum pump system is started until the pressure reaches a level of 1×10^{-5} mbar. Then the laser is turned on and

Die approbierte gedruckte Originalversion dieser Diplomarbeit ist an der TU Wien Bibliothek verfügbar
The approved original version of this thesis is available in print at TU Wien Bibliothek.

aligned to a position where the "1,2" mode is expected to have a high amplitude. Then the lock-in amplifier is used to find the specific resonance frequency and to lock it. Afterwards the oscillation amplitude can again be observed while the laser position is adjusted until an optimal position is reached. Once the laser is aligned to the resonator, the same procedure of recording the ring down and measuring the thermomechanical noise peak is performed to calibrate the system (see section 1.3). Once calibrated, the appropriate drive is applied and the frequency stability is recorded for 1 minute.

2.5 FTIR Measurement Setup

As an application of the implemented optical lever readout, FTIR combined with NEMS was chosen. FTIR uses infrared light to obtain information about materials in the infrared spectrum. In contrast to the regular operation, the variation implemented in this work uses NEMS resonators as both the detector and the sample. The modulated infrared light is directed onto the resonator, where some of the light is absorbed due to the interaction with molecular bonds in the material. This absorption induces a frequency shift in the resonator, which directly corresponds to the infrared absorption of the sample. By precisely recording this frequency shift and feeding it back to the FTIR via an external detector module, the FTIR can perform an FFT on the signal to obtain the corresponding infrared absorption spectrum. Instead of just using the resonator itself as the sample, analytes can also be deposited on the resonator in small quantities. This additional analyte then also absorbs infrared light at specific wavenumbers and passes this heat onto the resonator, which again causes the frequency of the resonator to shift. The FTIR device used in this work is the Bruker VERTEX 70, while the resonator setup is identical to the magnetomotive readout technique and optical lever technique setup respectively. The major difference is that the previously unused optical port on the bottom of the vacuum chamber has now the light from the FTIR passing through a diamond window (Diamond Materials GmbH & Co. KG). The diamond material allows infrared light to pass through to the underside of the resonator. Figure 2.8 illustrates the FTIR measurement setup.

Die approbierte gedruckte Originalversion dieser Diplomarbeit ist an der TU Wien Bibliothek verfügbar
The approved original version of this thesis is available in print at TU Wien Bibliothek.
TU Bibliothek Your knowledge hub WIEN

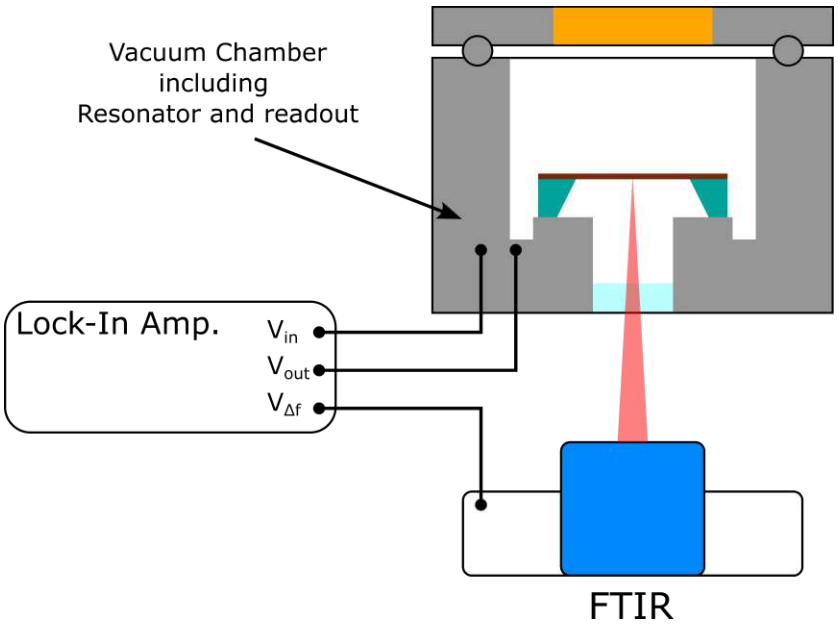

Figure 2.8: Measurement setup for FTIR spectroscopy with NEMS. Independent of readout technique the setup has the light source of the FITR pointed to the underside of the resonator and the measured frequency shift is fed back into the FTIR.

Die approbierte gedruckte Originalversion dieser Diplomarbeit ist an der TU Wien Bibliothek verfügbar
The approved original version of this thesis is available in print at TU Wien Bibliothek.

Chapter 3

Results

Die approbierte gedruckte Originalversion dieser Diplomarbeit ist an der TU Wien Bibliothek verfügbar
The approved original version of this thesis is available in print at TU Wien Bibliothek.

3.1 Allan Variance

To determine the effect of the read-out method on the frequency stability, it is essential to use the same NEMS device in identical or nearly identical environmental conditions as a basis for comparison. Consequently, all compared results were recorded under conditions that were kept as consistent as possible. Therefore, the same resonance mode was measured with the exact same resonators with each separate read-out technique. Since the frequency stability of the resonators is under investigation, it is important to also consider the devices used to record the frequency stability measurements. The lock-in amplifier and the PLL implement filters with low-pass functionalities, which must be taken into account as they suppress signals above a certain frequency. In this work, the low-pass filter bandwidth of the lock-in demodulation is set to $f_{\text{demod}} = 2.5\,\text{kHz}$ and the PLL bandwidth is set to $f_{\text{PLL}} = 500\,\text{Hz}$ for all measurements. Consequently, frequency fluctuations faster than the cutoff time $\tau_{\text{PLL}} = 2 \cdot 10^{-4}\,\text{s}$ are suppressed due to the low-pass behavior of the PLL. Since the thermal time constant of the resonators ($\tau_{\text{th}} = 30 \cdot 10^{-3}\,\text{s}$) limits the frequencies the resonators can follow, the PLL cutoff must be chosen to be faster than this thermal time constant. However, since this work also aims to investigate general detection noise, a larger-than-necessary PLL bandwidth was chosen.

3.1.1 Optical Lever vs Laser Vibrometer

The resonators used for this comparison, were five identical 1 mm square silicon nitride (SiN) membranes (see Chapter 2.1) with no electrodes. Although it was not feasible to employ identical vacuum chambers and for both methods, steps were taken to ensure the environments were as similar as possible. The drive amplitude and laser power are crucial for a proper comparison, as both significantly affect the performance and frequency stability of the resonator. While higher laser power can improve the signal-to-noise ratio, it also results in more energy being absorbed by the resonator, which then impacts the frequency stability due to thermal fluctuations. Thus, optimizing

Die approbierte gedruckte Originalversion dieser Diplomarbeit ist an der TU Wien Bibliothek verfügbar
The approved original version of this thesis is available in print at TU Wien Bibliothek.

the laser power is essential.
For this purpose after the first resonator was installed and ready to be measured, according to section 2.2.2 and section 2.4.1 respectively, the laser power was varied and for each power level one frequency stability measurement was recorded. So starting from the highest power setting, 1 min of frequency fluctuations were recorded for each power level. After each recording the power setting was reduced by one level and the system was allowed to stabilize for 5 min to not have the previous measurement influence the following one. These recordings were then analyzed to compute the Allan deviation, which helped identify the most effective power settings. This was done for both the LDV and OLT individually.
Figures 3.1 and 3.2 show the effect of an increase in laser power on the frequency stability of the resonator. For low power measurements, the detection noise is significantly higher than for high power measurements, which shows as a higher level of noise in the shorter integration times. But when increasing the laser power, there comes a turning point where, while the detection noise continues to decrease, the laser power fluctuations begin to impact the resonator and the frequency stability for larger integration times gets worse. Consequently, the laser power of the optical lever technique (OLT) was set to 100 µW, while the laser power of the laser Doppler vibrometer (LDV) was adjusted to 16 µW.

Die approbierte gedruckte Originalversion dieser Diplomarbeit ist an der TU Wien Bibliothek verfügbar
The approved original version of this thesis is available in print at TU Wien Bibliothek.

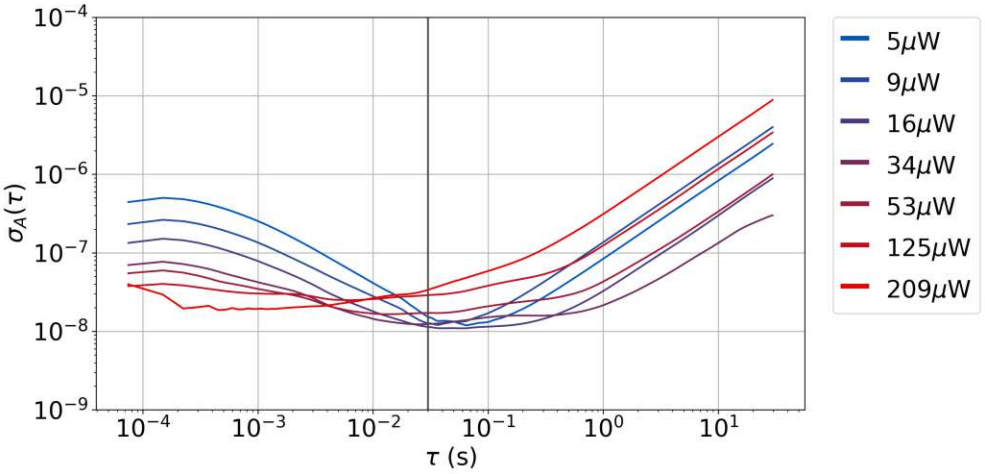

Figure 3.1: Allan deviations of the "S1" resonator for different power levels recorded on the LDV. The black vertical line marks the thermal time constant of the resonator at 30 ms.

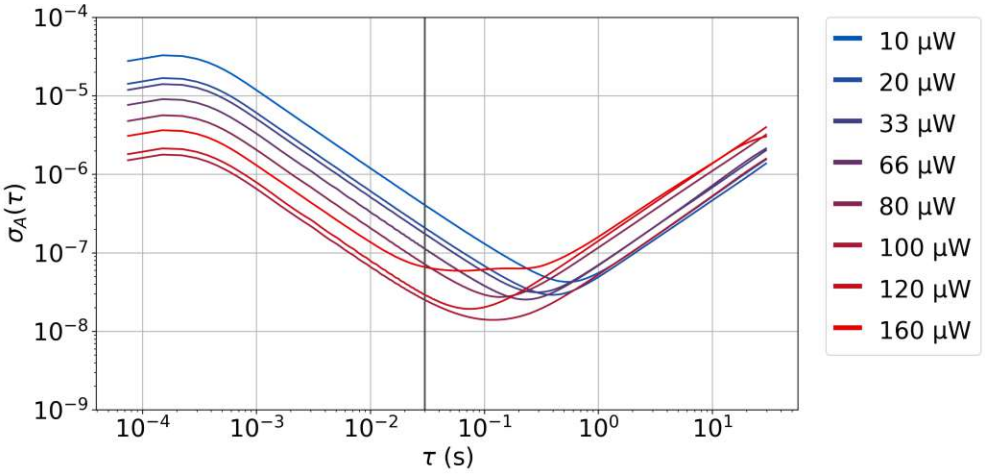

Figure 3.2: Allan deviations of the "S1" resonator for different power levels recorded with the OLT. The black vertical line marks the thermal time constant of the resonator at 30 ms.

After this power calibration, each resonator was measured respectively in each system with the now fixed power levels. The Allan deviations obtained

Die approbierte gedruckte Originalversion dieser Diplomarbeit ist an der TU Wien Bibliothek verfügbar
The approved original version of this thesis is available in print at TU Wien Bibliothek.

are shown in Figure 3.3.

Die approbierte gedruckte Originalversion dieser Diplomarbeit ist an der TU Wien Bibliothek verfügbar
The approved original version of this thesis is available in print at TU Wien Bibliothek.

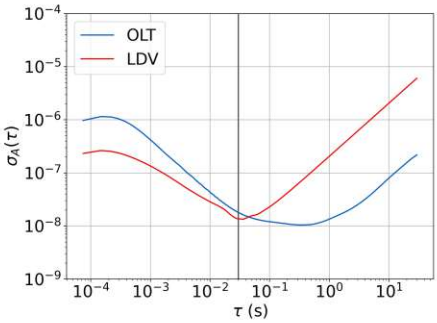

(a) Resonator S1

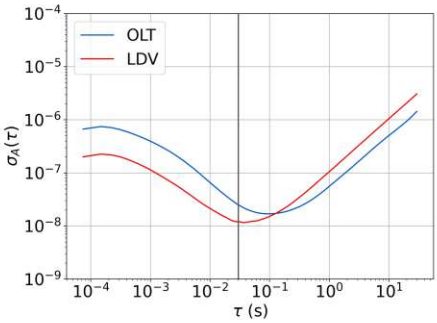

(b) Resonator S2

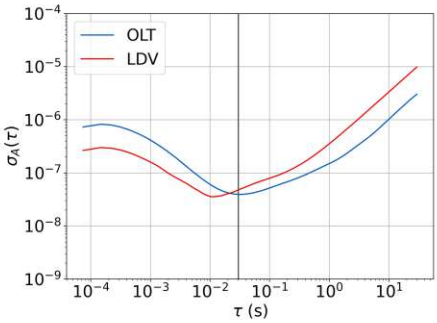

(c) Resonator S3

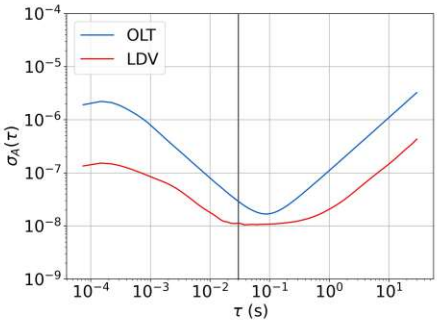

(d) Resonator S4

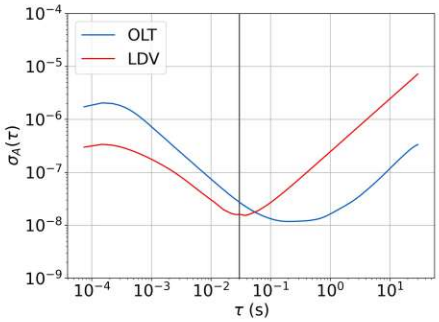

(e) Resonator S5

Figure 3.3: The measured Allan deviations for resonator S1 to S5 both with the OLT and the LDV. The black vertical line marks the thermal time constant of the resonator at 30 ms.

Die approbierte gedruckte Originalversion dieser Diplomarbeit ist an der TU Wien Bibliothek verfügbar
The approved original version of this thesis is available in print at TU Wien Bibliothek.
TU Bibliothek Your knowledge hub WIEN

The LDV shows a lower detection noise in the region of 1×10^{-4} s to 1×10^{-2} s, where not only is the Allan deviation itself lower, but also its slope is $\frac{1}{\sqrt{\tau}}$ compared to the optical lever technique, which scales with $\frac{1}{\tau}$. This indicates a lower electronic noise due to optimized electronics and their noise sources. However, given that the resonators in use have a thermal time constant of about 30 ms, this improvement is not significant for a measurement with these particular resonator. The resonators are not able to follow signals below their thermal time constant since their temperature simply does not adjust fast enough. In the 1×10^{-2} s to 1×10^{-1} s range, the performance of the OLT nearly matches that of the LDV, with only a factor of 2-5 difference. Beyond this range, up to end of the plot at 1×10^{2} s the OLT shows better noise performance, which can be attributed to an increased temperature drift in the LDV setup.

Two measurements that stand out are the measurement of resonator "S1" for the OLT and resonator "S4" for the LDV. Both exhibit a distinct flat section in their Allan deviation between 1×10^{-2} s and 1 s, this brings back the issue of laser power fluctuations and photothermal backaction [17, 18].
The Allan deviations for these two measurements indicate that the power responsivity of the resonators was high enough for laser fluctuations to manifest in their frequency stability. Since the laser power was set only once for all resonators, variations in individual resonator responses were not accounted for.
Figures 3.4 and 3.5, respectively, show the Allan deviation of resonators "S4" and "S1" individually. With sufficient knowledge of the resonator parameters and measurement setup, Kanellopulos et al. demonstrates that the frequency behavior of resonators can be largely grouped into three categories [18]. Equation (3.1) shows that the additive phase noise power spectral density (PSD) of a resonator $S_{\gamma_\theta}(\omega)$ consists of the thermomechanical noise PSD $S_{y_{\theta_{thm}}}(\omega)$ and the detection noise PSD $S_{y_{\theta_{det}}}(\omega)$.

$$S_{y_\theta}(\omega) = S_{y_{\theta_{thm}}}(\omega) + S_{y_{\theta_{det}}}(\omega) \tag{3.1}$$

Die approbierte gedruckte Originalversion dieser Diplomarbeit ist an der TU Wien Bibliothek verfügbar
The approved original version of this thesis is available in print at TU Wien Bibliothek.
TU Bibliothek Your knowledge hub WIEN

The additive phase noise PSD $S_{y_\theta}(\omega)$ combined with the PSD of noise due to temperature fluctuations $S_{y_{th}}(\omega)$ and the PSD of the noise due to the photothermal back action $S_{y_{\delta P}}(\omega)$ form the total noise PSD $S_y(\omega)$ as shown in Equation (3.2).

$$S_y(\omega) = S_{y_\theta}(\omega) + S_{y_{th}}(\omega) + S_{y_{\delta P}}(\omega) \tag{3.2}$$

By measuring the output light of the laser with an external power meter (Thorlabs S120VC) and converting the power fluctuations to frequency fluctuations via the power responsivity of the specific resonator, the effect laser power has on the resonator can be more accurately understood. The PSD of the frequency fluctuations caused by variations in laser power, $S_{y_{\delta P}}$, is shown in Figures 3.4 and 3.5, demonstrating good agreement with the measured data.

In retrospect, it seems feasible to record the power fluctuations first, and calculate the maximum suitable power of the laser source based on the responsivity of the structure to prevent the impact due to the laser source.

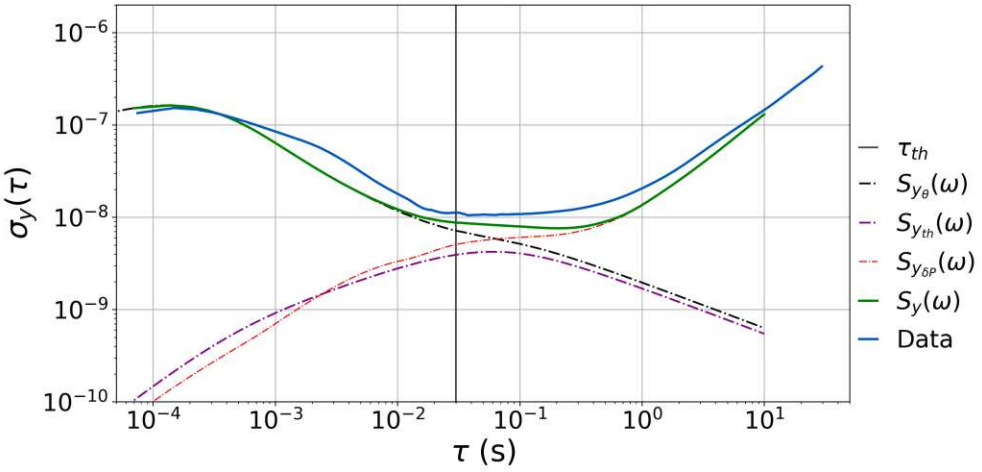

Figure 3.4: Allan deviation of resonator "S4" (blue) recorded with the LDV. The different noise contributions for the resonator are displayed individually and as their sum are displayed. τ_{th} indicates the thermal time constant of the resonator

.

Die approbierte gedruckte Originalversion dieser Diplomarbeit ist an der TU Wien Bibliothek verfügbar
The approved original version of this thesis is available in print at TU Wien Bibliothek.

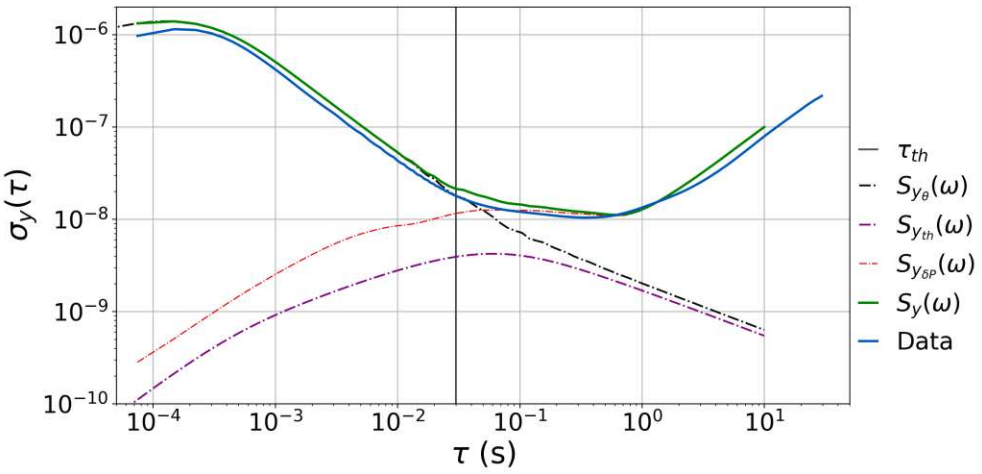

Figure 3.5: Allan deviation of resonator "S4" (blue) recorded with the OLT. The different noise contributions for the resonator are displayed individually and as their sum are displayed. τ_{th} indicates the thermal time constant of the resonator

.

As a last comparison between the LDV and the OLT, the transduction coefficient (see section 1.3), that was also used in the calibration, is compared for each chip. This is shown in Figure 3.6.

Die approbierte gedruckte Originalversion dieser Diplomarbeit ist an der TU Wien Bibliothek verfügbar
The approved original version of this thesis is available in print at TU Wien Bibliothek.

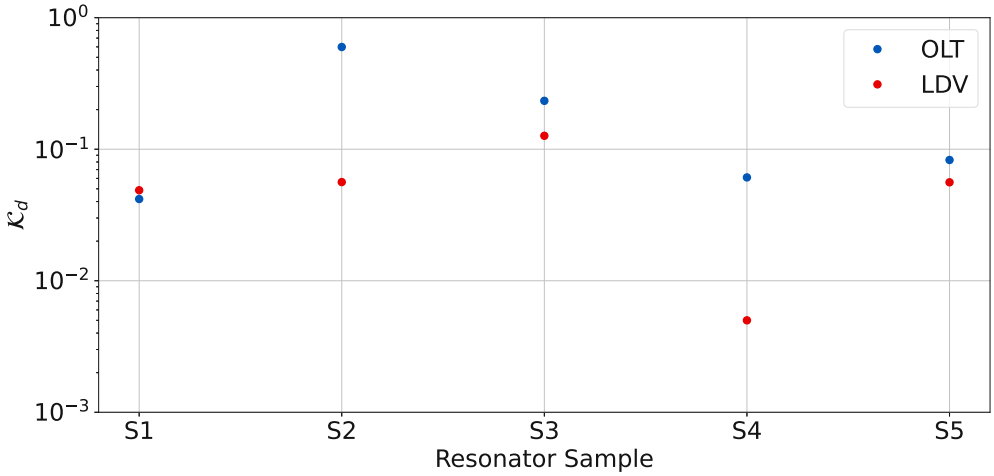

Figure 3.6: The extracted transduction coefficient for both the LDV and OLT for all five samples

The transduction coefficient depends on the read-out setup, its detection noise and the resonator itself. According to Bešić et al., the transduction coefficient is a limiting factor in the read-out of high-Q resonators [6]. Therefore, it was important in this work to demonstrate the capabilities of the optical lever technique in achieving transduction coefficients comparable to those of an LDV. Figure 3.6 shows that the two optical read-out methods exhibit very similar transduction coefficients for the resonators "S1", "S3" and "S5" while the measurements for "S2" and "S4" show a difference of around one magnitude. One possible reason for the inconsistency between the read-outs and between the resonators is that the data rate used for recording the thermomechanical noise PSD, which serves as the basis for the transduction coefficient, was not chosen high enough. A higher data rate and averaging across multiple measurements might yield more consistent results.

3.1.2 Optical Lever vs Magnetomotive

In this study the OLT was also compared with the magnetomotive read-out (MAG). The chamber used for both measurements allows for switching between magnetomotive and optical read-outs with minimal adjustments,

Die approbierte gedruckte Originalversion dieser Diplomarbeit ist an der TU Wien Bibliothek verfügbar
The approved original version of this thesis is available in print at TU Wien Bibliothek.

ensuring similar conditions for the resonators and a fair comparison, without having to move the resonator itself.

Three resonators of identical design were analyzed with both read-out systems, which since the magnetomotive read-out requires it to, have electrodes on top of the membrane. For the OLT, the laser was again calibrated by measuring the Allan deviation at various laser power levels and selecting the setting that provided the most stable results. In Figure 3.7 is it apparent that the power level of 150 mW performed the best, as it shows the lowest overall detection noise without introducing additional fluctuations. The reason for the increase in laser power, in comparison to the measurements done with the pure silicon nitride membranes (without electrodes), is that the additional gold absorbs some of the heat and helps conduct it off of the membrane, allowing for more laser power to be used on these resonators.

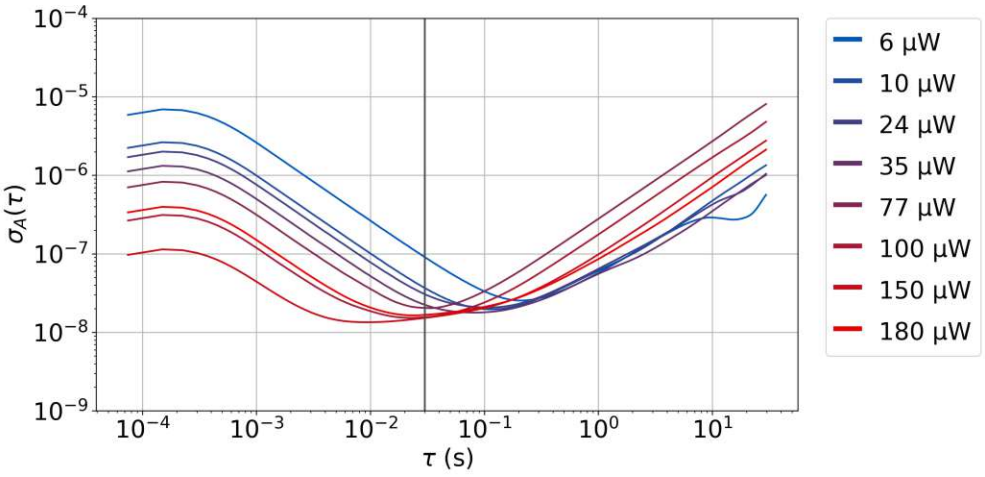

Figure 3.7: Allan deviations of the "S7" resonator for different power levels recorded with the OLT. The black vertical line marks the thermal time constant of the resonator at 30 ms.

Due to the presence of additional gold electrodes on the resonator, which alter their characteristics compared to bare structures, the system was not calibrated via the theoretical critical amplitude. At the same time the magnetomotive read-out is not able to resolve thermomechanical noise peaks,

Die approbierte gedruckte Originalversion dieser Diplomarbeit ist an der TU Wien Bibliothek verfügbar
The approved original version of this thesis is available in print at TU Wien Bibliothek.

therefore a calibration of this read-out is not possible at all. Instead, actuation was based on the frequency response, where the locked frequency of the resonator is observed while adjusting the drive. The critical amplitude is defined as the threshold amplitude before non-linear affects significantly show up in the frequency stability [15]. This can be observed by increasing the drive of a locked resonator, since if the non-linear regime is reached, the frequency shifts even though only the drive was changed. When the drive is reduced, the frequency decreases again to the previous value. Using this as an indicator makes it possible to approximate the critical amplitude, which was how the two systems were compared in this work. Each resonator was first installed with the magnetomotive setup, locked, the resonator was driven close to the critical amplitude and the frequency stability was measured. Then the setup was changed to the OLT setup which just involved removing the electrical connections that connected to the chip and installing the optical setup of the OLT on top of the vacuum chamber. The chip was otherwise not moved to ensure a good comparison. The calculated Allan deviations are displayed in Figure 3.8 and indicate a significant difference in noise characteristics. This was expected since this time it is not a comparison between two optical read-out techniques like the LDV and the OLT, but rather an electrical read-out with an optical read-out.

Die approbierte gedruckte Originalversion dieser Diplomarbeit ist an der TU Wien Bibliothek verfügbar
The approved original version of this thesis is available in print at TU Wien Bibliothek.

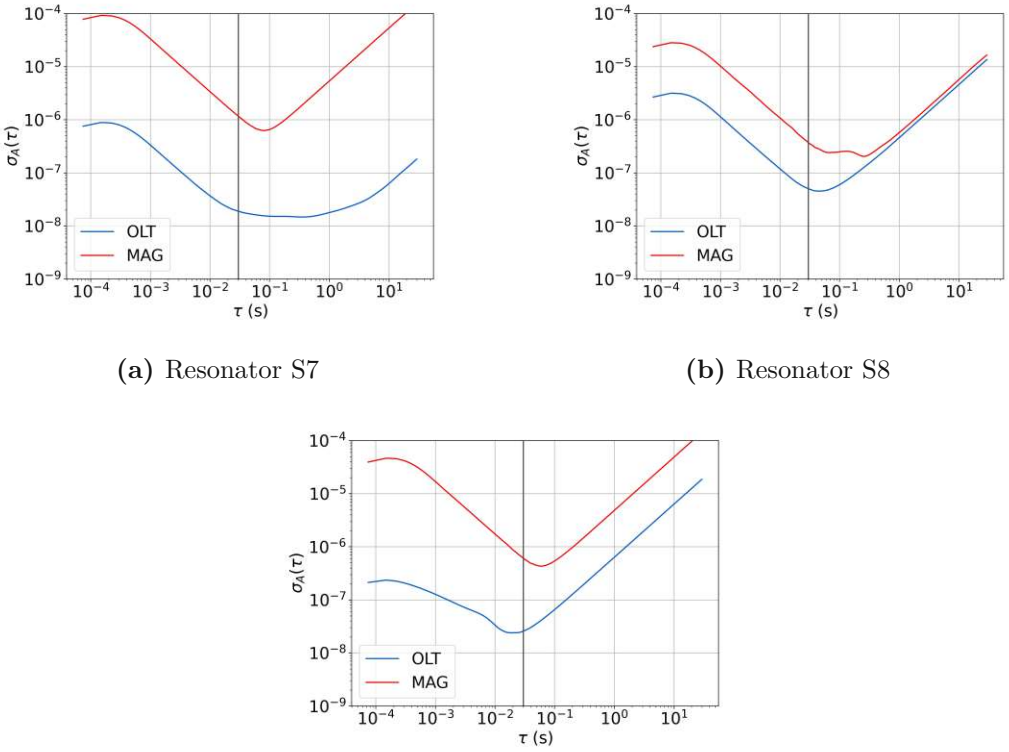

(a) Resonator S7

(b) Resonator S8

(c) Resonator S9

Figure 3.8: The measured Allan deviations for resonator S7 to S9 both with the OLT and the magnetomotive read-out. The black vertical line marks the thermal time constant of the resonator at 30 ms.

The OLT measurements for resonator "S7" and "S9" show an improvement in detection noise of about two magnitudes and the measurement of "S8" still shows an improvement of about one magnitude. This is due to the additional noise the electronic read-out introduces compared to an optical measurement technique like the OLT. Noise in the actuation as well as read-out directly affects the resonator and therefore, its frequency stability.

Die approbierte gedruckte Originalversion dieser Diplomarbeit ist an der TU Wien Bibliothek verfügbar
The approved original version of this thesis is available in print at TU Wien Bibliothek.

3.2 FTIR Spectra

Infrared spectroscopy uses the infrared spectrum of light to characterize analytes based on their absorption spectra. This method can be implemented with NEMS devices, where the analyte is deposited on the resonator. The frequency shifts caused by the absorption of light via the particles are tracked and fed into the FTIR device. The setup for this is depicted in Figure 2.8.

To compare the magnetomotive and optical readout techniques, polypropylene (PP) nanoparticles were deposited on a membrane resonator via spray deposition [29]. These nanoparticles are 50 nm polypropylene (PP50 Lab261) spheres and PP is a material with a very characteristic infrared spectrum. The nanoparticles absorb light at specific wavelengths, causing the resonator to heat up due to the absorbed energy. However, the resonator material (silicon nitride) itself also absorbs infrared light. To mitigate the effects of unwanted absorption by the resonator, a background measurement was performed without the nanoparticles on the resonator. This background spectrum is later subtracted from the spectrum recorded with the nanoparticles to obtain a spectrum of the added analyte only.

Identical measurements were carried out using both the magnetomotive and the optical lever technique for both the background measurement as well as the resonator with analyte. The process of recording a spectrum with an FTIR starts with recording an interferogram, which is later transformed via the FFT to a spectrum via the FTIR device.
The interferogram of the empty chip recorded with the two techniques is shown in Figure 3.9. Especially in the close-up regions in Figure 3.9 b-d), it becomes apparent that the noise performance of the two read-outs directly shows in the interferogram. The magnetomotive read-out shows additional noise on top of the signal, compared to the optical lever technique. The interferograms recorded with the analyte-loaded resonator (Fig. 3.10) contain frequency information from both the empty resonator and the analyte, resulting in a superimposed signal. Consequently, the signal-to-noise ratio is

Die approbierte gedruckte Originalversion dieser Diplomarbeit ist an der TU Wien Bibliothek verfügbar
The approved original version of this thesis is available in print at TU Wien Bibliothek.
TU Bibliothek Your knowledge hub WIEN

reduced compared to the interferogram of the empty resonator. Despite this, the magnetomotive read-out still exhibits additional noise compared to the optical lever technique. It is hard to create a metric for quantifying the noise in an interferogram due to the mix between signal and noise. Both components have a wide range in frequencies and no direct way to distinguish them.

Die approbierte gedruckte Originalversion dieser Diplomarbeit ist an der TU Wien Bibliothek verfügbar
The approved original version of this thesis is available in print at TU Wien Bibliothek.
TU Bibliothek Your knowledge hub WIEN

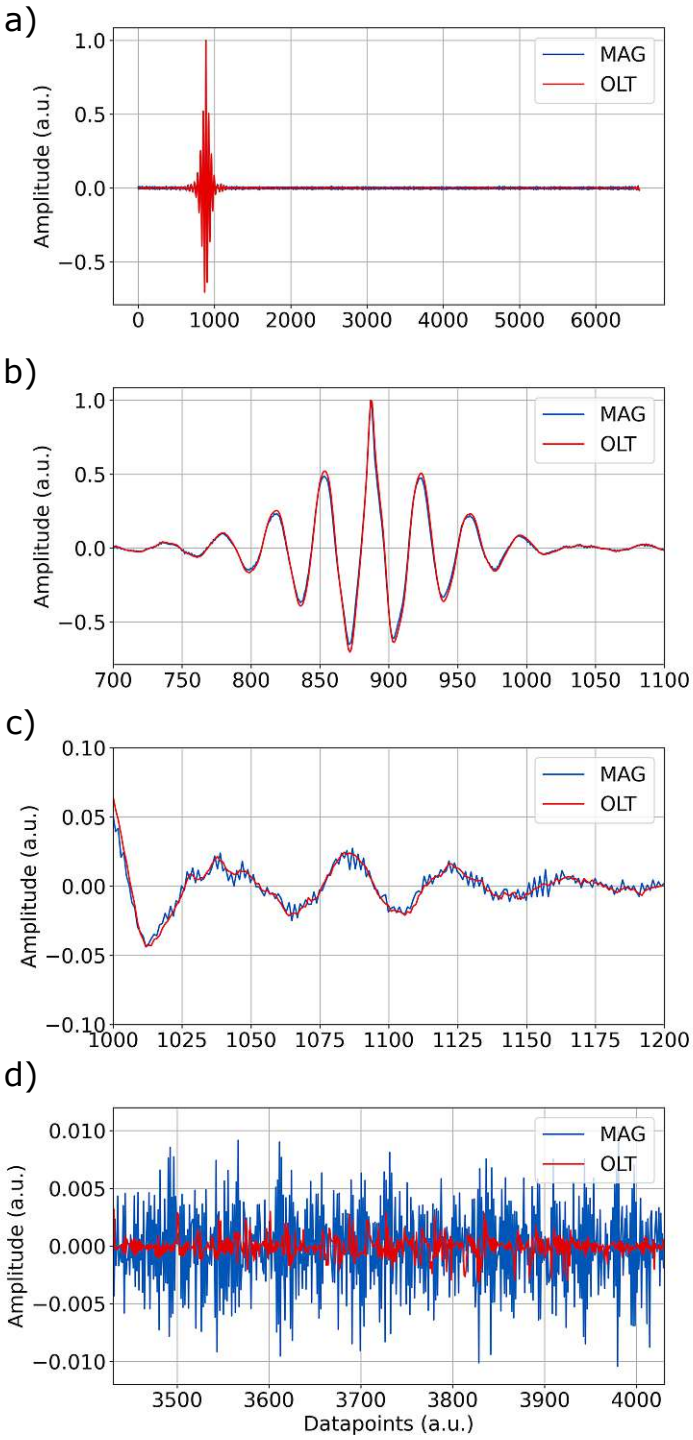

Figure 3.9: Interferograms of an empty resonator without analyte, recorded using the magnetomotive (MAG) and optical lever (OLT) techniques. a) shows the full interferogram. b-d) show close-ups of regions in the interferograms.

Die approbierte gedruckte Originalversion dieser Diplomarbeit ist an der TU Wien Bibliothek verfügbar
The approved original version of this thesis is available in print at TU Wien Bibliothek.

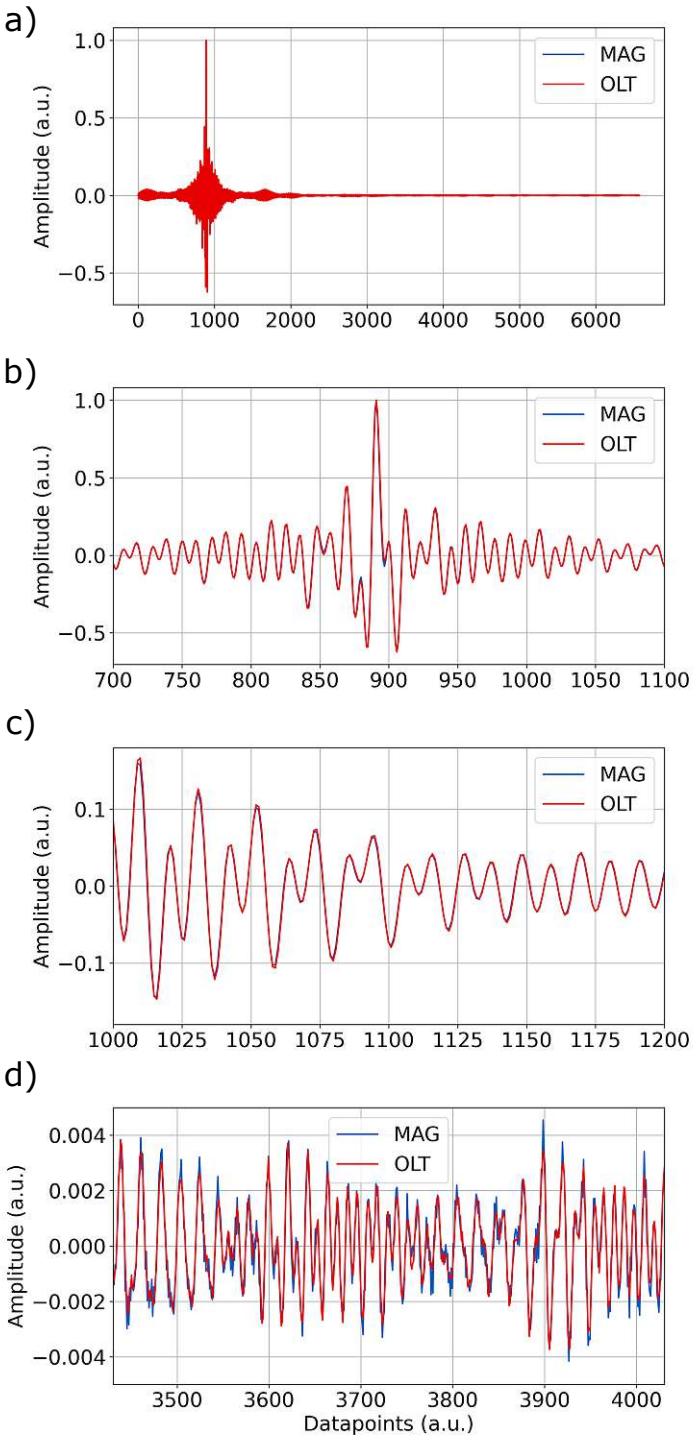

Figure 3.10: Interferograms of a resonator with PP particles, recorded using the magnetomotive (MAG) and optical lever (OLT) techniques. a) shows the full interferogram. b-d) show close-ups of regions in the interferograms.

Die approbierte gedruckte Originalversion dieser Diplomarbeit ist an der TU Wien Bibliothek verfügbar
The approved original version of this thesis is available in print at TU Wien Bibliothek.

After the interferograms are processed by the FTIR device, the spectral information becomes visible and the corresponding spectra can be studied. One metric of interest is the signal-to-noise (SNR) of a spectrum. For this work, the ratio of a particular spectral intensity was compared to the standard deviation of a region with no spectral features (see equ. (3.3)).

$$SNR = \frac{S}{\sigma} \tag{3.3}$$

The empty resonator (see fig. 3.11) exhibits a prominent absorption peak around $840\,\mathrm{cm}^{-1}$ and otherwise shows almost no spectral features. This peak represents the absorption of the silicon nitride material of the resonator, which is largely transparent at most wavelengths except in the range around $840\,\mathrm{cm}^{-1}$.

Die approbierte gedruckte Originalversion dieser Diplomarbeit ist an der TU Wien Bibliothek verfügbar
The approved original version of this thesis is available in print at TU Wien Bibliothek.
TU Bibliothek Your knowledge hub WIEN

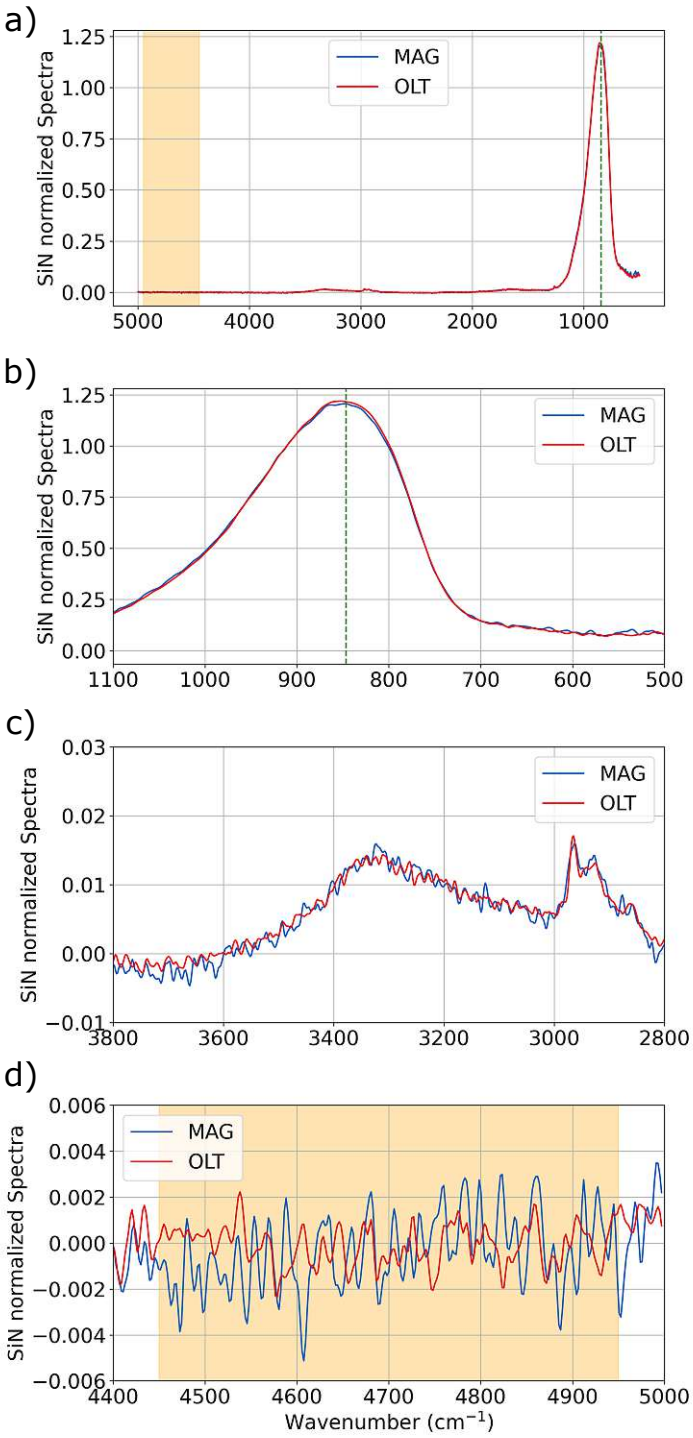

Figure 3.11: Infrared spectra of an empty resonator without analyte, based on the interferogram recorded using the magnetomotive (MAG) and optical lever (OLT) techniques. a) shows the full spectra. b-d) show close-ups of regions of the spectra. The orange region indicates the noise region and the green line the signal for the SNR

Die approbierte gedruckte Originalversion dieser Diplomarbeit ist an der TU Wien Bibliothek verfügbar
The approved original version of this thesis is available in print at TU Wien Bibliothek.

	Signal	Noise σ [10^{-6}]	SNR (a.u.)
MAG	1.21	1600	754
OLT	1.22	865	1409

Table 3.1: Extracted values and SNR of the spectra of an empty resonator recorded with the MAG and the OLT.

To calculate the SNR and compare the two spectra, this peak was selected as the representative signal in the SNR calculation (see fig. 3.11a-b)). The noise was determined based on the standard deviation within the wavenumber region indicated in Figure 3.11a),d).

Table 3.1 presents the extracted values and the calculated SNR for the empty resonator. While the peak amplitude is similar due to normalization, the noise level of the magnetomotive read-out is nearly twice as high as that of the optical read-out, resulting in an SNR that is almost half for the electrical read-out.

The spectra of the resonator with PP particles deposited on it show many more spectral features and to isolate the spectra of the analyte, the previously recorded background spectra, shown in Figure 3.11, is subtracted from it. The resulting background-corrected spectra is shown in Figure 3.12 and does no longer show the peak corresponding to the silicon nitride. The particles cause several sharp absorption peaks in the infrared spectrum. The wavenumbers of these peaks match well with wavenumbers found in literature [37–39].

Die approbierte gedruckte Originalversion dieser Diplomarbeit ist an der TU Wien Bibliothek verfügbar
The approved original version of this thesis is available in print at TU Wien Bibliothek.
TU Bibliothek Your knowledge hub WIEN

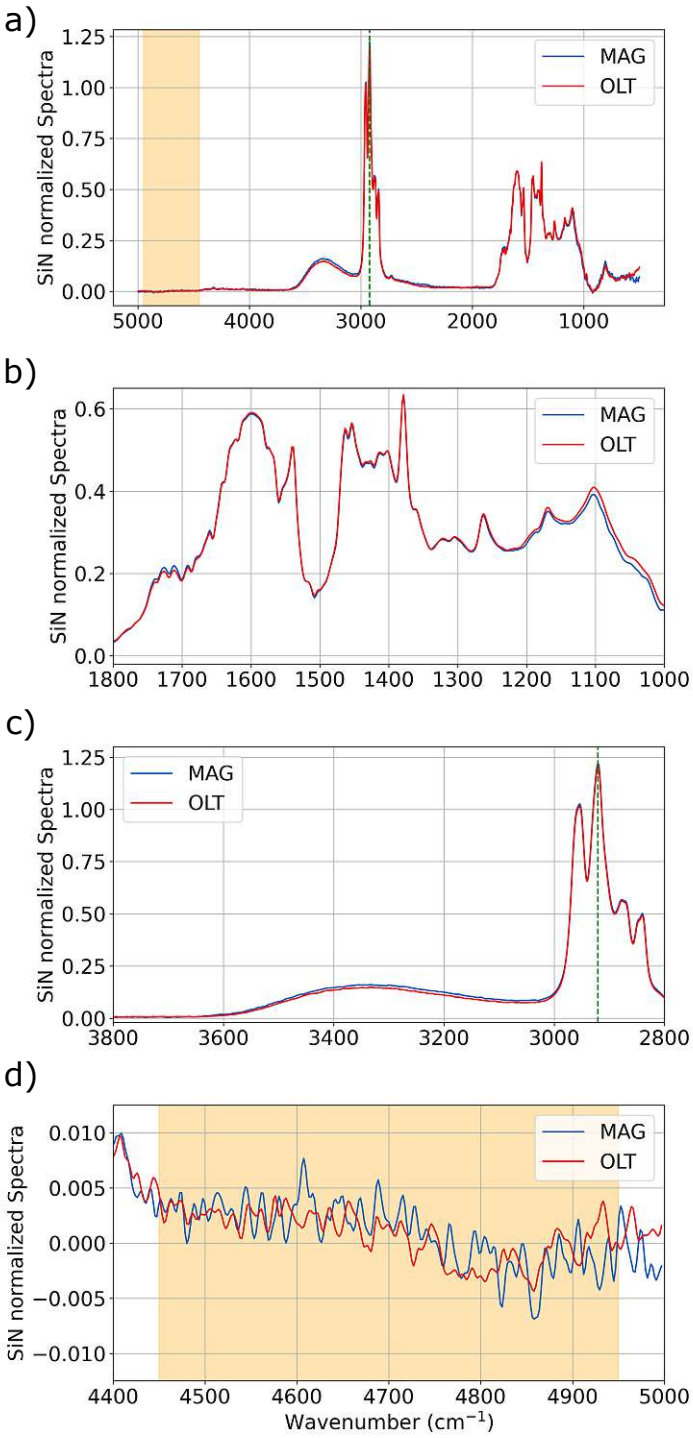

Figure 3.12: Infrared spectra of a resonator with PP particles, based on the the interferogram recorded using the magnetomotive (MAG) and optical lever (OLT) techniques. a) shows the full spectra. b-d) show close-ups of regions of the spectra. The orange region indicates the noise region and the green line the signal for the SNR

Die approbierte gedruckte Originalversion dieser Diplomarbeit ist an der TU Wien Bibliothek verfügbar
The approved original version of this thesis is available in print at TU Wien Bibliothek.

	Signal	Noise σ [10^{-6}]	SNR (a.u.)
MAG	1.22	2756	443
OLT	1.21	2180	553

Table 3.2: Extracted values and SNR of the spectra of a resonator with PP particles recorded with the MAG and the OLT.

For the SNR of these spectra, the same noise region as before for the empty resonator was chosen. But since this spectra now represents the analyte a, representative peak for polypropylene at 2920 cm^{-1} was selected. Based on the intensity of this peak as the signal and the standard deviation of the noise region as the noise, the SNR can again be calculated for both spectra (see tab. 3.2).

In comparison the SNR of the spectra recorded with the OLT still shows a better noise performance, but in comparison to the SNR corresponding to the empty resonator, the noise decreased drastically for both read-outs. Still the OLT shows a higher SNR compared to the MAG.

Compared to the results obtained in section 3.1, the difference between MAG and OLT is less apparent. Even for the spectra of the empty resonator, the difference in SNR is just a factor of two. This can be explained to the techniques an FTIR device uses to calculate the spectra from the time signal. Due to the FFT and several processing steps, the noise of the time signal does no linearly affect the resulting spectra. One could compare the noise that is contained in the interferogram, since this is a time signal and suffering from the same noise, that also the frequency stability measurements in section 3.1 experienced. The problem why this is not trivial is the superposition of signal and noise in the interferogram. Because the interferogram contains frequency information of a wide range of frequencies, it is hard to interpret what compromises the signal and what is just noise.

The results presented in this section show the application of the optical lever technique as well as the magnetomotive read-out and their impact on the spectra obtained via FTIR. The SNR based on the empty resonator as well as the one based on the resonator with particles, show a clear improvement for the optical read-out over the electrical one.

Die approbierte gedruckte Originalversion dieser Diplomarbeit ist an der TU Wien Bibliothek verfügbar
The approved original version of this thesis is available in print at TU Wien Bibliothek.
TU Bibliothek Your knowledge hub WIEN

Chapter 4

Conclusion

Die approbierte gedruckte Originalversion dieser Diplomarbeit ist an der TU Wien Bibliothek verfügbar
The approved original version of this thesis is available in print at TU Wien Bibliothek.

This work presented a comparative study of three read-out techniques—magnetomotive (MAG), optical lever technique (OLT), and laser Doppler vibrometry (LDV)—focusing on their noise performance and frequency stability. Additionally, FTIR measurements were conducted to evaluate the performance of MAG and OLT in a practical spectroscopy application.

The results demonstrate that the OLT setup offers noise performance comparable to LDV under certain conditions, confirming its viability as a read-out method for NEMS characterization. Its compact and straightforward design enhances its appeal for experimental setups requiring versatility and cost-effectiveness. However, further optimization of the system could improve its performance and usability. For instance, integrating a microcontroller or advanced electronic circuits to process all four quadrants simultaneously would eliminate the dependence of the read-out on the bending orientation of the resonator.

A key focus of this study was the transduction coefficient, a critical parameter in high-Q resonator read-outs. The results confirm that, for most cases, the OLT achieves transduction coefficients comparable to LDV, although some inconsistencies in measurements indicate the need for further refinement in data acquisition and processing.

In the context of FTIR spectroscopy, the noise reduction achieved by the OLT over the magnetomotive method was clearly visible in both the interferogram and the extracted spectrum. While Fourier transformation reduces the impact of time-domain noise, the optical read-out still exhibited an overall improvement. Furthermore, the optical technique eliminates the need for electrodes, reducing fabrication complexity and enabling multiple resonators to be measured within a vacuum chamber by simply repositioning the laser. This provides a clear advantage over the electrical method, particularly in terms of scalability and cost reduction.

Overall, this study successfully demonstrates the feasibility of using the optical lever technique for NEMS resonators in a vacuum environment, providing a non-contact, low-cost alternative to traditional optical methods such as LDV. The findings contribute to the broader exploration of alternative transduction mechanisms in nanoscale mechanical sensing, paving the way

Die approbierte gedruckte Originalversion dieser Diplomarbeit ist an der TU Wien Bibliothek verfügbar
The approved original version of this thesis is available in print at TU Wien Bibliothek.
TU Bibliothek Your knowledge hub WIEN

for more adaptable and optimized sensing technologies in fundamental research and practical applications.

Die approbierte gedruckte Originalversion dieser Diplomarbeit ist an der TU Wien Bibliothek verfügbar
The approved original version of this thesis is available in print at TU Wien Bibliothek.
TU Bibliothek Your knowledge hub WIEN

Bibliography

[1] A.T-H. Lin et al. “Methods for enhanced electrical transduction and characterization of micromechanical resonators”. *Sensors and Actuators A: Physical* 158.2 (2010), pp. 263–272 (cit. on p. 1).

[2] Andreas Barg et al. “Measuring and imaging nanomechanical motion with Laser Light”. *Applied Physics B* 123.1 (Dec. 2016) (cit. on p. 1).

[3] A. N. Cleland and M. L. Roukes. “Fabrication of high frequency nanometer scale mechanical resonators from bulk si crystals”. *Applied Physics Letters* 69.18 (Oct. 1996), pp. 2653–2655 (cit. on pp. 1, 41).

[4] M. Belov et al. “Mechanical resonance of clamped silicon nanowires measured by optical interferometry”. *Journal of Applied Physics* 103.7 (Apr. 2008) (cit. on p. 1).

[5] R. W. Andrews et al. “Bidirectional and efficient conversion between microwave and Optical Light”. *Nature Physics* 10.4 (Mar. 2014), pp. 321–326 (cit. on p. 1).

[6] Hajrudin Bešić et al. “Schemes for tracking resonance frequency for micro- and nanomechanical resonators”. *Physical Review Applied* 20.2 (Aug. 2023) (cit. on pp. 1, 10, 11, 13, 16, 17, 55).

[7] K. L. Ekinci and M. L. Roukes. “Nanoelectromechanical systems”. *Review of Scientific Instruments* 76.6 (May 2005), p. 061101 (cit. on p. 1).

[8] R V Jones. “Some developments and applications of the optical lever”. *Journal of Scientific Instruments* 38.2 (Feb. 1961), pp. 37–45 (cit. on p. 1).

Die approbierte gedruckte Originalversion dieser Diplomarbeit ist an der TU Wien Bibliothek verfügbar
The approved original version of this thesis is available in print at TU Wien Bibliothek.
TU Bibliothek Your knowledge hub WIEN

[9] Nicholas A. Geisse. "AFM and combined optical techniques". *Materials Today* 12.7 (2009), pp. 40–45 (cit. on p. 1).

[10] Ke Bian et al. "Scanning probe microscopy". *Nature Reviews Methods Primers* 1.1 (May 2021) (cit. on p. 1).

[11] Alexandre Dazzi and Craig B. Prater. "AFM-IR: Technology and Applications in Nanoscale Infrared Spectroscopy and Chemical Imaging". *Chemical Reviews* 117.7 (2017). PMID: 27958707, pp. 5146–5173 (cit. on p. 1).

[12] Jonathan D. Adams et al. "High-speed imaging upgrade for a standard sample scanning atomic force microscope using small cantilevers". *Review of Scientific Instruments* 85.9 (Sept. 2014) (cit. on p. 1).

[13] Constant A.J. Putman et al. "A theoretical comparison between interferometric and optical beam deflection technique for the measurement of cantilever displacement in AFM". *Ultramicroscopy* 42-44 (1992), pp. 1509–1513 (cit. on p. 1).

[14] Shan Hao and Thomas P. Purdy. "Back action evasion in optical lever detection". *Optica* 11.1 (Jan. 2024), p. 10 (cit. on p. 1).

[15] Silvan Schmid, Luis Guillermo Villanueva, and Michael Lee Roukes. *Fundamentals of Nanomechanical Resonators*. Springer International Publishing AG, 2023 (cit. on pp. 3, 5, 8, 10, 12, 13, 19, 20, 22, 23, 30, 39, 41, 57).

[16] Enrico Rubiola and François Vernotte. "The companion of enrico's chart for phase noise and two-sample variances". *IEEE Transactions on Microwave Theory and Techniques* 71.7 (July 2023), pp. 2996–3025 (cit. on pp. 8, 10).

[17] Pedram Sadeghi et al. "Frequency fluctuations in nanomechanical silicon nitride string resonators". *Phys. Rev. B* 102 (21 Dec. 2020), p. 214106 (cit. on pp. 10, 11, 52).

Die approbierte gedruckte Originalversion dieser Diplomarbeit ist an der TU Wien Bibliothek verfügbar
The approved original version of this thesis is available in print at TU Wien Bibliothek.
TU Bibliothek Your knowledge hub WIEN

[18] Kostas Kanellopulos et al. “Comparative analysis of nanomechanical resonators: Sensitivity, response time, and practical considerations in Photothermal Sensing”. *Microsystems & Nanoengineering* 11.1 (Feb. 2025) (cit. on pp. 11, 52).

[19] *About Lock-In Amplifiers*. Accessed on 10.05.2024. URL: https://www.thinksrs.com/downloads/pdfs/applicationnotes/AboutLIAs.pdf (cit. on pp. 14, 15).

[20] Roland E. Best. *Phase-locked loops: Design, simulation, and applications*. McGraw-Hill, 2011 (cit. on p. 16).

[21] Constant A. Putman et al. “A detailed analysis of the optical beam deflection technique for use in atomic force microscopy”. *Journal of Applied Physics* 72.1 (July 1992), pp. 6–12 (cit. on p. 19).

[22] Stephen D. Senturia. *Microsystem design*. Springer US, 2001 (cit. on p. 23).

[23] Savas Ozdemir et al. “Measuring the Quality Factor in MEMS Devices”. *Micromachines* 6.12 (2015), pp. 1935–1945 (cit. on p. 23).

[24] Min-Hang Bao. *Analysis and design principles of MEMS devices*. Elsevier, 2005 (cit. on p. 23).

[25] Eric M. Lawrence, Kevin E. Speller, and Duli Yu. “MEMS characterization using laser Doppler vibrometry”. *SPIE Proceedings* (Jan. 2003) (cit. on p. 25).

[26] S.J. Rothberg et al. “An international review of Laser Doppler vibrometry: Making light work of vibration measurement”. *Optics and Lasers in Engineering* 99 (Dec. 2017), pp. 11–22 (cit. on p. 25).

[27] Miao-Hsuan Chien et al. “Single-molecule optical absorption imaging by nanomechanical photothermal sensing”. *Proceedings of the National Academy of Sciences* 115.44 (2018), pp. 11150–11155 (cit. on p. 26).

[28] Kostas Kanellopulos, Robert G. West, and Silvan Schmid. “Nanomechanical Photothermal Near Infrared Spectromicroscopy of Individual Nanorods”. *ACS Photonics* 10.10 (2023), pp. 3730–3739 (cit. on p. 26).

Die approbierte gedruckte Originalversion dieser Diplomarbeit ist an der TU Wien Bibliothek verfügbar
The approved original version of this thesis is available in print at TU Wien Bibliothek.
TU Bibliothek Your knowledge hub WIEN

[29] Niklas Luhmann et al. “Nanoelectromechanical infrared spectroscopy with in situ separation by thermal desorption: NEMS-ir-TD”. *ACS Sensors* 8.4 (Apr. 2023), pp. 1462–1470 (cit. on pp. 26, 29, 41, 59).

[30] Alexandre Dazzi et al. “AFM–IR: Combining Atomic Force Microscopy and Infrared Spectroscopy for Nanoscale Chemical Characterization”. *Applied Spectroscopy* 66.12 (2012). PMID: 23231899, pp. 1365–1384 (cit. on p. 26).

[31] Brian C. Smith. *Fundamentals of fourier transform infrared spectroscopy*. CRC Press, 2011 (cit. on p. 27).

[32] Jonathan D. Adams et al. “High-speed imaging upgrade for a standard sample scanning atomic force microscope using small cantilevers”. *Review of Scientific Instruments* 85.9 (Sept. 2014) (cit. on p. 31).

[33] Accessed on 01.06.2024. URL: https://www.edmundoptics.com/knowledge-center/application-notes/optics/understanding-waveplates/ (cit. on p. 33).

[34] Raoul Enning et al. “A high frequency sensor for optical beam deflection atomic force microscopy”. *Review of Scientific Instruments* 82.4 (Apr. 2011) (cit. on p. 35).

[35] Accessed on 02.06.2024. URL: https://www.analog.com/en/resources/technical-articles/stabilize-transimpedance-amplifier-circuit-design.html (cit. on p. 35).

[36] Markus Piller et al. “Thermal IR Detection With Nanoelectromechanical Silicon Nitride Trampoline Resonators”. *IEEE Sensors Journal* 23.2 (2023), pp. 1066–1071 (cit. on p. 41).

[37] Peltzer M and Catherine Simoneau. *Report of an interlaboratory comparison from the European Reference Laboratory for Food Contact : ILC002 2013 - Identification of polymeric materials*. Jan. 2013 (cit. on p. 65).

Die approbierte gedruckte Originalversion dieser Diplomarbeit ist an der TU Wien Bibliothek verfügbar
The approved original version of this thesis is available in print at TU Wien Bibliothek.
TU Bibliothek Your knowledge hub WIEN

[38] Nancy González-Canché et al. “Evaluation of surface treatments on 5052-H32 aluminum alloy for enhancing the interfacial adhesion of thermoplastic-based fiber metal laminates”. *International Journal of Adhesion and Adhesives* 82 (Apr. 2018), pp. 90–99 (cit. on p. 65).

[39] Aravinthan Gopanna et al. “Fourier transform infrared spectroscopy (FTIR), Raman spectroscopy and wide-angle X-ray scattering (WAXS) of polypropylene (PP)/cyclic olefin copolymer (COC) blends for qualitative and quantitative analysis”. *Polymer Bulletin* 76.8 (Nov. 2018), pp. 4259–4274 (cit. on p. 65).

Die approbierte gedruckte Originalversion dieser Diplomarbeit ist an der TU Wien Bibliothek verfügbar
The approved original version of this thesis is available in print at TU Wien Bibliothek.